





Seasonality of Mesoscale Phytoplankton Control in Eastern Fram Strait

Vibe Schourup-Kristensen^{1,2} , Claudia Wekerle¹ , Sergey Danilov^{1,3} , and Christoph Völker¹ 

¹Alfred-Wegener-Institut Helmholtz Zentrum für Polar und Meeresforschung, Bremerhaven, Germany, ²Now at Department of Bioscience, Aarhus University, Roskilde, Denmark, ³Department of Mathematics and Logistics, Jacobs University, Bremen, Germany

Key Points:

- Eddy-resolving model run shows strong dependence of Fram Strait chlorophyll distribution on the mesoscale eddy field
- During the spring bloom, chlorophyll is highest in areas of positive vorticity, associated with a shallow mixed layer and convergence
- In late the summer, chlorophyll is highest in areas of negative vorticity, associated with nutrient upwelling and doming nutriclines

Correspondence to:

V. Schourup-Kristensen,
vibe.schourup@bios.au.dk

Citation:

Schourup-Kristensen, V., Wekerle, C., Danilov, S., & Völker, C. (2021). Seasonality of mesoscale phytoplankton control in eastern Fram Strait. *Journal of Geophysical Research: Oceans*, 126, e2021JC017279. <https://doi.org/10.1029/2021JC017279>

Received 13 FEB 2021

Accepted 8 AUG 2021

Abstract Globally, mesoscale processes create a rich and filamented pattern in biological productivity. Despite of remoteness and a harsh environment, observations likewise show an impact of mesoscale processes on phytoplankton growth in the Arctic. Observations of sufficiently high resolution are, however, difficult to carry out. Large-scale models are another way to gain knowledge about the system. In the current study, we use a global sea ice-ocean biogeochemical model, which is eddy resolving in Fram Strait, to show that the mesoscale dynamics has a strong effect on shaping phytoplankton growth. For the year 2009, we demonstrate that the growth season in the West Spitzbergen Current can be divided into two regimes; during Regime I, which takes place in May and June before and during the spring bloom, high chlorophyll concentrations are associated with areas of positive vorticity and a shallow mixed layer, pointing toward light limitation controlling growth. During Regime II, which occurs after the bloom from mid-July to late August, the highest chlorophyll concentration is found in areas of negative vorticity. Here, upwelling of nutrient-rich water occurs, through doming isopycnals, acting to raise the nutricline, may also play a role in alleviating nutrient limitation in the surface water. The study suggests that the mesoscale eddy environment locally modulates the seasonal cycle of light and nutrient limitation. Knowledge of the eddy field should be taken into consideration for making conclusions from point-wise measurements in Fram Strait.

Plain Language Summary Fram Strait is the main gateway to the Arctic Ocean, where cold and fresh Arctic water meets warm and salty Atlantic water. Eddies are continuously generated in the area, producing a swirling pattern, and stirring of water masses. In this study, we use a global model with high resolution in Fram Strait, including sea ice, ocean, and biology. We show that phytoplankton is strongly dependent on the rotating motion of the surface water, creating a rich imprint of rotation on the phytoplankton concentration. Further, we show that this dependence changes through summer. Before and during the spring bloom, filaments with a shallow mixed layer have the highest chlorophyll concentration, pointing toward alleviation of light limitation being important for phytoplankton growth. In late summer, when nutrients are limiting productivity in the surface water, the chlorophyll concentration is elevated in areas where nutrients are brought upwards from deeper water. The alleviation of light and nutrient limitation occurs through different processes, making the phytoplankton growth shift from one type of rotating filament to another as the summer progresses. The study tells us that knowledge about the horizontal patchiness of phytoplankton should be taken into consideration for analyses of in-situ data in Fram Strait.

1. Introduction

Being the main oceanographic gateway to the Arctic Ocean, Fram Strait has been the site of continuous monitoring of physical and biological parameters for more than 20 years in the form of scientific cruises and permanent mooring stations (e.g., Nöthig et al., 2020; Soltwedel et al., 2016). The area is highly dynamical, with the topographically steered, northward flowing, West Spitzbergen Current (WSC) transporting relatively warm and salty Atlantic Water into the Arctic Ocean (Beszczynska-Moller et al., 2012). Conversely, the East Greenland Current (EGC), which is covered by a semipermanent ice tongue, brings colder and fresher Polar Water southward in western Fram Strait (de Steur et al., 2009), thereby creating a strong zonal gradient of properties across the strait. Despite of challenging conditions with regards to for example,

© 2021 The Authors.

This is an open access article under the terms of the [Creative Commons Attribution-NonCommercial License](https://creativecommons.org/licenses/by-nc/4.0/), which permits use, distribution and reproduction in any medium, provided the original work is properly cited and is not used for commercial purposes.

weather and ice, eddies have been found to be ubiquitous across the Arctic Ocean (e.g., Carpenter & Timmermans, 2012; Kozlov et al., 2019; Pnyushkov et al., 2018), and are thought to be significant in shaping the general circulation (Timmermans & Marshall, 2020). In Fram Strait, mesoscale eddies have been observed in the open water as well as the marginal ice zone since the 1980s (Gascard et al., 1988; Johannessen et al., 1987). Eddies are shed from the WSC, and facilitate mixing between the water masses of the WSC and the EGC, as they transport properties of the WSC northwestward across Fram Strait. Using numerical linear stability analysis of a mooring array in the WSC, Teigen et al. (2010, 2011) showed that the instabilities are especially strong during late winter and spring. Data from these moorings confirmed that the eddy kinetic energy (EKE) is three times stronger in late winter compared to late summer (von Appen et al., 2016).

Knowledge of mesoscale control of biology in the Arctic Ocean is, however, lacking, though an increasing number of studies suggest that small-scale processes indeed are important drivers for biological productivity (Frajka-Williams et al., 2009; Marchese, 2018; Nishino et al., 2018), in line with studies from other world oceans (e.g., Mahadevan et al., 2012; Uchida et al., 2020). High-resolution satellite-based chlorophyll images (Liu et al., 2018) and model runs (Schourup-Kristensen et al., 2018) show a variable and filamentous imprint on the spatial chlorophyll distribution in Fram Strait. Additionally, despite of logistical challenges, in situ observations likewise indicate that the complex frontal dynamics shapes the distribution of biological properties in Fram Strait (Fadeev et al., 2021; Wulff et al., 2016). A filamented pattern of biological properties, created by mesoscale ocean dynamics, has been observed across the global ocean in, for example, ocean color images (e.g., Gaube et al., 2013; Mahadevan et al., 2012; McGillicuddy, 2016), and in ocean-scale model runs (e.g., Lévy et al., 2014). Depending on local conditions, such as nutrient availability, light levels, and ecosystem composition, this spatial imprint can occur due to localized nutrient pulses to a nutrient depleted euphotic zone, driven by strong vertical velocities along mesoscale fronts (Ramachandran et al., 2014; Uchida et al., 2020). Another mechanism is localized shoaling or deepening of the mixed layer, contributing to modulating the depth of the euphotic zone and thus affecting for instance the timing of the spring bloom (Brody et al., 2016; Mahadevan et al., 2012; Olita et al., 2014). Subduction of particulate organic matter is a third mechanism, which has been suggested in model studies to affect the biological properties in the ocean (Omand et al., 2015; Watanabe et al., 2014). Cyclonic/anti-cyclonic eddies, characterized by a core of positive and negative vorticity, respectively, and anti-clockwise/clockwise rotation (Northern Hemisphere), affect the vertical nutrient supply through for example, down- and upwelling (Martin & Richards, 2001) and upward/downward displacement of the pycnocline resulting in shallow/deep anomalies of the mixed layer (Dufois et al., 2014; Hausmann et al., 2017).

A common trait of these mechanisms is that they occur in a three-dimensional domain. This, combined with their transient nature, makes it complicated to sample in the field and it makes it difficult to quantify the processes driving the interactions between physics and biology.

Productivity in Fram Strait is predominantly light limited early in the year, with phytoplankton growth being induced in late spring, when ice melt and solar heating act to stratify the upper water column (Cherkasheva et al., 2014; Rey et al., 2000). The bloom maximum occurs in June (Nöthig et al., 2015). As the nutrients in the surface water become depleted, the phytoplankton growth follows the downward movement of the nutricline, and a subsurface chlorophyll maximum develops (Cherkasheva et al., 2013). The growth season lasts for a total of ~120 days (Nöthig et al., 2015). The complex physical environment of Fram Strait, combined with the northerly location, leads to large variability of biological properties in space and time (e.g., Fadeev et al., 2021; von Appen et al., 2018; Wulff et al., 2016). But, so far, it has not been possible to carry out studies on the scale necessary to assess the physical mechanisms driving the variability, neither with in situ observations, ocean color measurements or model calculations.

A number of eddy permitting model studies of the Arctic Ocean physics have been carried out (e.g., Chen et al., 2016; Dupont et al., 2015; Wekerle, Wang, Danilov, et al., 2017), but the added model and computational complexity of biogeochemistry means that only a few eddy permitting model runs include biology (Schourup-Kristensen et al., 2018; Watanabe et al., 2014). These runs are carried out on meshes with a resolution of 4.5 km, not enough to resolve eddies in Fram Strait, where the first baroclinic radius of deformation is on the order of 4–6 km (von Appen et al., 2016). Using unstructured meshes, eddy resolving model runs focusing on Fram Strait have only been carried out in recent years (Hattermann et al., 2016; Wekerle, Wang, von Appen, et al., 2017), highlighting that resolving eddies in Fram Strait is critical in order to

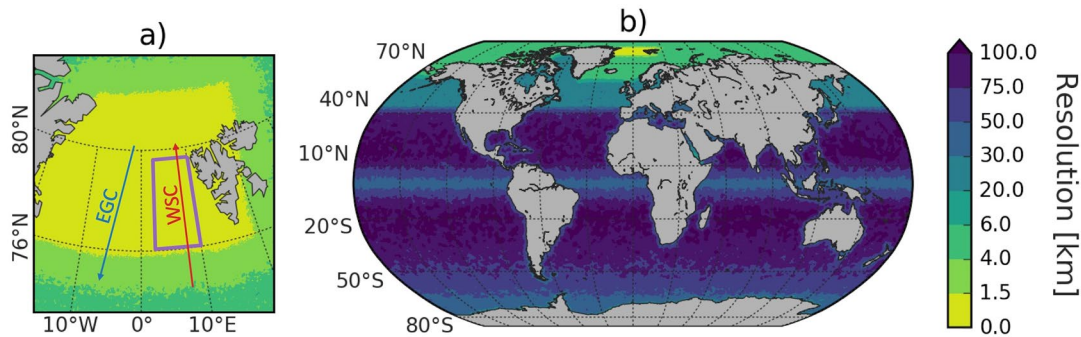


Figure 1. Horizontal resolution of the model grid. (a) Zoom of Fram Strait with the West Spitzbergen Current (WSC) and the East Greenland Current (EGC) marked with a blue and red arrow, respectively. The purple square marks the study area. (b) The global mesh.

realistically represent the physical circulation, and especially the return flow of Atlantic Water in the area. So far, however, nobody has run a model with sufficiently high resolution to study the mesoscale effects of eddies on the phytoplankton in the area.

In this study, we explore the impact of the mesoscale variability on the spatial chlorophyll distribution in Fram Strait. Further, we look into the seasonal change of the mesoscale imprint on light and nutrient limitation, and thus phytoplankton growth. We do this by using the biogeochemical model REcoM2 (Schourup-Kristensen et al., 2014) coupled to the Finite Element Sea ice-Ocean Model (FESOM, Wang et al., 2014; Wekerle, Wang, von Appen, et al., 2017), and running it in a global setup which is eddy resolving in Fram Strait.

2. Method

2.1. Model Setup

For this study, the Regulated Ecosystem Model (REcoM2, Schourup-Kristensen et al., 2014), was run in a global setup, coupled to the multi-resolution Finite Element Sea ice-Ocean Model (FESOM, Wang et al., 2014). REcoM2 is a biogeochemical model with three nutrients (nitrate, silicate, and iron), two phytoplankton classes (diatoms and nanophytoplankton) and one class of zooplankton and detritus. The model employs variable stoichiometry, allowing the phytoplankton C:N, C:Chl, and N:Si ratios to adapt, depending on nutrient availability and light conditions (Geider et al., 1998). Light limitation is controlled by the light availability and the phytoplankton Chl:C ratio. Nutrient uptake limitation is controlled by Michaelis-Menten kinetics, while nutrient growth limitation depends on the intracellular N:C and Si:C ratios, and temperature as described in Schourup-Kristensen et al. (2014). Zooplankton grazing is parameterized by a sigmoidal prey function (Gentleman et al., 2003). FESOM-REcoM2 has been used for, for example, global carbon studies (Friedlingstein et al., 2020; Hauck et al., 2020), and the multi-resolution capabilities have been utilized to carry out an eddy-permitting Arctic setup, which the current study builds upon (Schourup-Kristensen et al., 2018).

The sea ice-ocean model, FESOM, solves the hydrostatic primitive equation in the Boussinesq approximation using finite element discretization (Wang et al., 2014). Consequently, calculations are carried out on an unstructured triangulated mesh in the horizontal domain, making it possible to increase resolution in dynamically important areas (Chassignet et al., 2020; Sidorenko et al., 2020) and areas of interest in the study at hand (e.g., Nakayama et al., 2020). FESOM has been used extensively to carry out model runs with a horizontal resolution of up to 1 km in the Arctic Ocean, making it possible to study for example, the mesoscale field in Fram Strait (Wekerle et al., 2020), the dynamics of the sea ice leads (Wang et al., 2016), and the distribution of plastic pollution in the Arctic (Tekman et al., 2020).

In the current study, we use a mesh with a horizontal resolution of 1 km in Fram Strait (from 76° to 82°N, Figure 1a), 4.5 km in the remainder of the Arctic Ocean north of 60°N and lower in the rest of the world (Figure 1b). In Fram Strait, the first baroclinic deformation radius is on the order of 5 km (von Appen et al., 2016; Nurser & Bacon, 2014), making this model run eddy resolving in the area, as was also

demonstrated by Wekerle, Wang, von Appen, et al. (2017). In the vertical, FESOM uses z-coordinates. The resolution is 10 m in the upper 100 m of the water column, and gradually decreases with depth.

Validation of modeled mesoscale features is a challenge due to the small spatial scale and transient nature of the eddies. The eddy field of this model run has been assessed against mooring observations, showing that hydrography and eddy kinetic energy was well captured in FESOM (Wekerle, Wang, von Appen, et al., 2017; Wekerle et al., 2020). To further evaluate the model run, FESOM's representation of eddies in Fram Strait has been compared to another eddy-resolving sea ice-ocean model, showing that for example, eddy life time, ratio of cyclonic to anti-cyclonic eddies, and size of eddies is similar in the two model runs (Wekerle et al., 2020), adding confidence that the models do a reasonable job in representing Fram Strait mesoscale features.

The physical model (FESOM) was spun up for 10 years, using the CORE-II atmospheric forcing for 2000–2009 (Large & Yeager, 2008). The year 2009 was then restarted, this time with the biogeochemical module (REcoM2) turned on. The coupled FESOM-REcoM2 run was carried out for one year, a similar time frame to other high-resolution Arctic studies (Watanabe et al., 2014). The global nutrient fields of REcoM2 (dissolved inorganic nitrate and silicate) were initialized with fields from World Ocean Atlas 2005 (Garcia et al., 2006), while dissolved iron was initialized with output from NEMO-PISCES (Aumont & Bopp, 2006) due to scarcity of iron measurements.

2.2. Eddy Detection

We distinguish between filaments and eddies with a closed core, by employing the Okubo-Weiss criterion (Okubo, 1970; Weiss, 1991). The Okubo-Weiss criterion (OW, Equation 1) defines eddies as areas where vorticity dominates over strain:

$$OW = \underbrace{(\delta_x u - \delta_y v)^2 + (\delta_x v + \delta_y u)^2}_{\text{Normal and shear component of strain}} - \underbrace{(\delta_x v - \delta_y u)^2}_{\text{Relative vorticity}} \quad (1)$$

An area is considered an eddy when the $OW < 0.2\sigma_{OW}$, where σ_{OW} is the spatial standard deviation of OW, and when the area has the same sign of vorticity (Isern-Fontanet et al., 2006).

3. Results

3.1. Structure of Surface Fields

Snapshots of relative vorticity ($\zeta^z = \delta_x v - \delta_y u$) normalized by the Coriolis parameter (f) and of sea surface temperature (SST) on June 1, 2009 (Figure 2) reveal a strong imprint of mesoscale activity, with well-defined closed vortices as well as interweaving filaments. This mesoscale imprint is especially strong in eastern Fram Strait, where the relatively warm and salty WSC water flows northward, shedding eddies that contribute to the return flow of the Return Atlantic Water (e.g., Wekerle, Wang, von Appen, et al., 2017). In the open water area between 76 and 79°N, the ratio between the relative vorticity and the coriolis parameter (ζ^z/f) ranges from -0.7 to 0.9 between April and September, indicating a strong ageostrophic component in the flow. The relative vorticity is damped in the southward flowing water mass below the ice in eastern Fram Strait (range of -0.4 – 0.5). In the open water as well as the ice covered area, there is a slight overweight of cyclonic eddies and filaments (Wekerle et al., 2020), as was also observed by Johannessen et al. (1987). The diameter of the eddies is on average 10 km (Wekerle et al., 2020).

The strong mesoscale activity acts to bring together water masses with different properties, thus creating strong horizontal gradients in the field of SST (Figure 2b), following the imprint of the vorticity (Figure 2a). In eastern Fram Strait, frontogenesis intensifies the vertical velocities along the edges of the anticyclonic filaments, thus bringing relatively warm subsurface water toward the surface, creating a tendency toward warmer water in areas of negative vorticity. The cyclonic eddies and filaments do, on the contrary, tend to be relatively cold due to the convergence of surface-cooled water occurring here. In the ice covered region of north-western Fram Strait, the effect of eddies on the SST distribution is much smaller due to the combination of a less strong eddy field, and a smaller vertical temperature gradient. The sea ice edge, on the other hand, is strongly modulated by the presence of submesoscale eddies. As the water warms, the thin ice edge

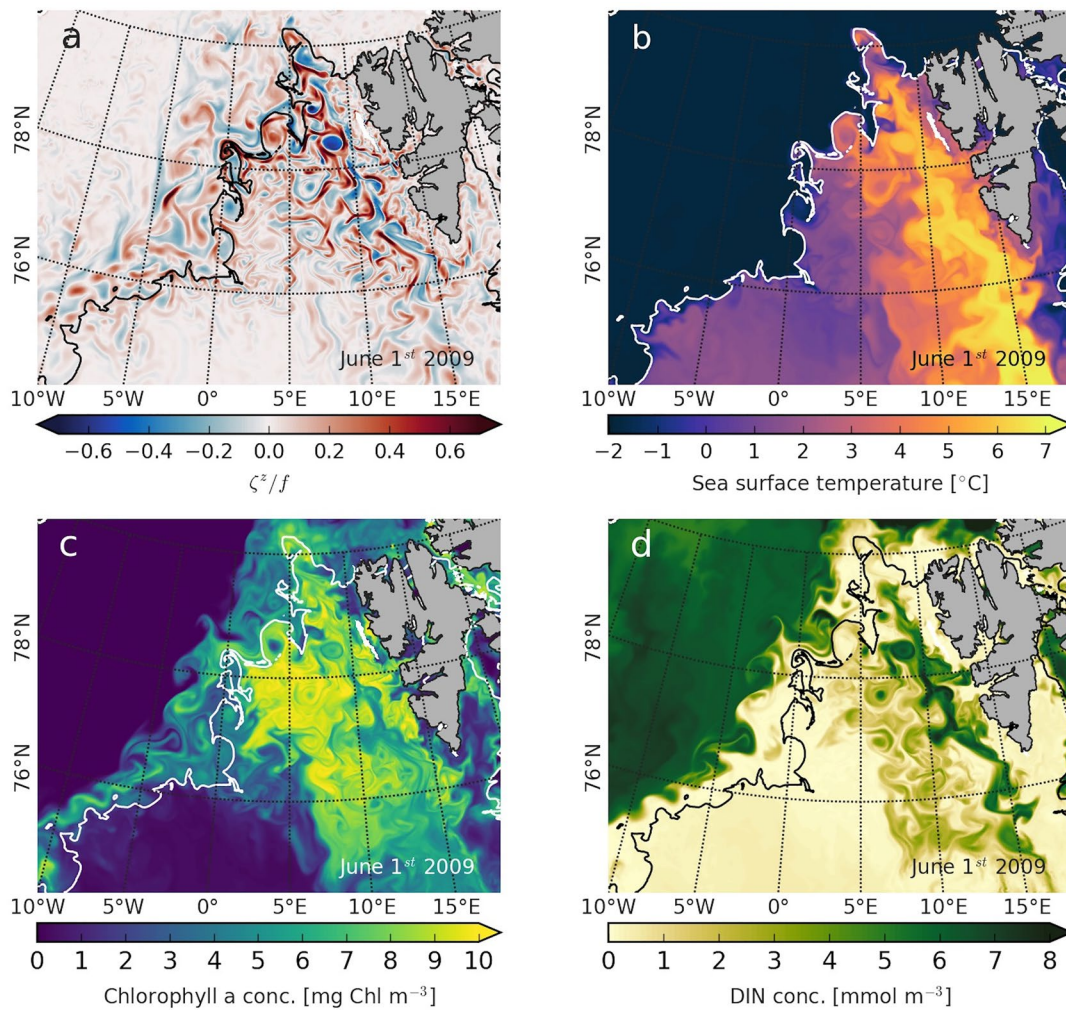


Figure 2. (a) Relative surface vorticity normalized by the Coriolis parameter, f , in Fram Strait. (b) Sea surface temperature. (c) Surface chlorophyll a concentration. (d) Surface concentration of dissolved inorganic nitrogen. The black/white lines mark the isoline of 10% ice concentration. All plots are model snapshots of June 1, 2009.

is deformed by the horizontal motion, creating a filamentous imprint along the ice edge, roughly following isolines of zero vorticity (Figure 2).

The biological productivity in Fram Strait is highly variable, in spatial as well as in temporal terms (Cherkasheva et al., 2013). On the 1st of June (Figure 2), the modeled spring bloom is at its highest, a timing of the bloom that is supported by ocean color images (e.g., Cherkasheva et al., 2014). On the kilometer-scale, the surface chlorophyll concentration in the model (Figure 2c) shows an even stronger likeness to the vorticity field than the SST does, a tendency also observed by Levy and Klein (2004). The imprint of the filamented flow is clear, with eddies showing up as circular chlorophyll filaments of alternately high and low concentration. Comparing the plot of the surface chlorophyll concentration to the plot of the relative vorticity, there is a tendency toward lower chlorophyll concentration in filaments of negative vorticity, for example, in the large north-south-going filament associated with the meandering WSC and associated eddies in eastern Fram Strait (Figure 2a), which show up as low-chlorophyll imprints in Figure 2c. These same areas tend toward higher SST than the surrounding water (Figure 2b) as well as higher dissolved inorganic nitrogen (DIN) concentrations (Figure 2d), indicating upwelling of nutrient-rich and warmer deep water, as would be expected in areas of negative vorticity. But, this relationship does not appear to hold across Fram Strait, and the connection between vorticity value and chlorophyll concentration will be further explored in the following sections. Looking at the larger scale distribution of the chlorophyll, the concentration is highest

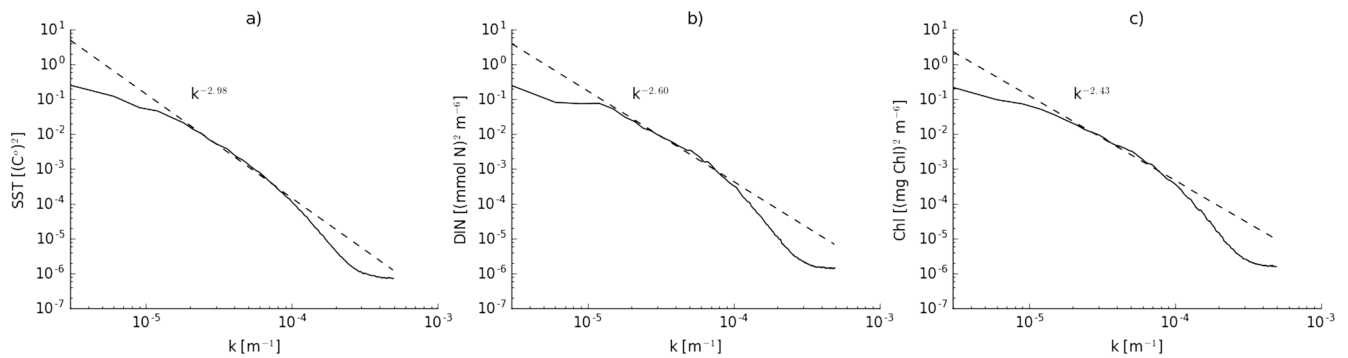


Figure 3. The mean power density spectra calculated from daily averaged values for north south sections in the West Spitzbergen Current (WSC) (a) sea surface temperature (SST) (b) dissolved inorganic nitrogen (DIN) (c) Chlorophyll (Chl).

in the WSC, and also elevated, although to a smaller degree, along the ice edge (Figure 2c). Further to the west, below the ice, productivity is very low, something that is mainly connected to lack of light, and we will not further discuss this area in the current manuscript. Both the ice edge and WSC area have relatively strong values of relative vorticity as compared to the ice-free areas of lower chlorophyll concentration, indicating that the vorticity field plays a role in modulating the physical and biochemical environment, and thereby also the large-scale distribution of chlorophyll. One effect of the mesoscale field is the elevation of surface DIN concentration in eastern Fram Strait (Figure 2d). Despite of chlorophyll and DIN appearing to be anti-correlated at this time, indicating that other factors act to control productivity, the upwelled DIN is spreading in the surface water, thereby indirectly sustaining productivity in eastern Fram Strait. In contrast, productivity is very low in the low vorticity and low DIN area of southern Fram Strait, further suggesting that the mesoscale forces sustain the bloom in other places.

3.2. Spectral Slopes

Calculating the power density spectra (PDS) for SST, surface chlorophyll and the surface DIN concentration, it is possible to quantitatively look into the contribution of different spatial scales to the total variance of the fields. The PDSs are calculated along north-south sections in the area between 4 and 10°E and 76–79°N. This area is located in the WSC, but avoids near shore areas and ice. Separate PSDs are calculated for each north-south section in the spatial fields, and for every second day of the main growth season in Fram Strait, from of May 1 to August 1. The final PSD is an average of these separate PSDs, and shows an approximate linear variation on a log-scale in the range from 10 to 100 km (a wave number of 10^{-5} to 10^{-4} m^{-1}). The spectrum slopes are calculated by applying linear regression to log-transformed values corresponding to this length scale. The mean spectral slope for SST is -2.98 , close to the value obtained by Capet et al. (2008), while the spectral slopes for DIN and chlorophyll are -2.60 and -2.43 , respectively. This is reasonably close to observed values (Martin & Srokosz, 2002). Overall, the slopes of the three spectra are very similar, indicating that they are all vary on the same spatial scales. Nevertheless, our modeled values for the spectral slopes decrease somewhat from SST over DIN to chlorophyll, showing a weakening mesoscale control. This weakening relationship has also been shown in other studies (Levy & Klein, 2004) and is due to DIN and chlorophyll not being passive tracers, with chlorophyll partly depending on the DIN concentration. Starting from the scales of about 10 km and decreasing (toward larger k), a spectral drop-off occurs, showing that numerical dissipation kicks in at these scales. This is a common property of numerical simulations and another explanation of why 1-km mesh is needed: on a coarser mesh, many eddies and filaments will be affected by build-in dissipation.

3.3. Temporal Shift in Vorticity-Chlorophyll Relationship

The similarities in the patterns of the spatial distribution of vorticity and the biological tracers (Figure 2), as well as the similar spectral slopes for SST, chlorophyll, and DIN (Figure 3), indicate that the spatial patchiness of chlorophyll and DIN concentration is driven by the mesoscale ocean dynamics. To further

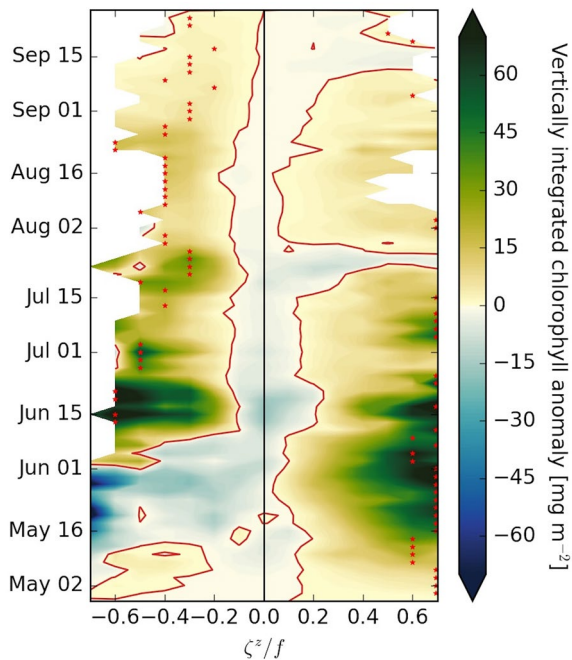


Figure 4. (a) Daily anomalies of vertically integrated chlorophyll concentration calculated in vorticity bins of width 0.1 for early May to mid-September, with values for every second day. The red stars mark the vorticity bin with the highest chlorophyll anomalies of the day in question. The red isolines mark zero anomaly. Calculations are carried out in the WSC (4 – 10°E and 76 – 79°N). Vertically integrated chlorophyll concentration is chosen, as the chl_{max} moves down in the water column as the growth season progresses.

investigate this relationship in the WSC (4 – 10°E and 76 – 79°N, the same area used to calculate spectra, Figure 3), we calculate the mean of vertically integrated chlorophyll concentration within vorticity bins with a width of 0.1, following Levy and Klein (2004). The anomaly is calculated by subtracting the daily average of the whole area from the average of each bin. The calculation does not take into account that the area associated with vorticity of small magnitude is larger than the area associated with a larger magnitude of vorticity. The percentage area within each bin is shown in Figure A1. The chlorophyll anomaly calculation is carried out for every model output (every second day) in the bloom season, lasting from early May to mid-September. The resulting diagram (Figure 4) shows that the chlorophyll concentrations increase with increasing vorticity values during the month of May, while a mirror-like pattern appears from June onwards, with the chlorophyll concentration increasing with both increasing positive and negative values of vorticity (Figure 4).

The location of the daily maximum of the chlorophyll anomaly, with respect to vorticity, further magnifies the tendency; from early May to mid-June, the highest chlorophyll anomalies occur in the bins centered around the positive vorticity values of 0.6 and 0.7. Next, from mid-June to mid-July, chlorophyll maximum alternates between bins of high negative and high positive values of relative vorticity. Finally, despite of the apparent mirror-like pattern of chlorophyll concentrations around zero vorticity, the chlorophyll maxima are located in bins of negative vorticity from mid-July to the end of August. During this last period, the chlorophyll maxima are located in vorticity bins with values ranging from –0.3 to –0.6. As the summer progresses, the relative vorticity in the model becomes weaker, especially for negative values, as illustrated by the increasingly wide areas of no data at the two vorticity extremes in Figure 4. This weakening is consistent with observations of EKE in the WSC, which has been shown to be strongest in late winter and weakest in late summer (von Appen et al., 2016).

The pattern of the chlorophyll anomalies and maxima indicates that a regime change takes place during summer; in the period from early May to mid-June productivity is mainly being induced in filaments of positive vorticity (In the following, we refer to this period as Regime I). Subsequently, the system moves toward an intermediate regime in which high values of both positive and negative vorticity is associated with high chlorophyll concentration. And finally, there is a stronger association between chlorophyll concentration and negative vorticity filaments than to positive vorticity filaments (Figure 4). In the following, we refer to this period as Regime II.

To explore the robustness of the relationship between chlorophyll and vorticity, we have calculated the correlation between chlorophyll and the absolute values of positive and negative vorticity, respectively, for every second day. For positive vorticity, this is done by masking out values larger than 0.1 in the WSC (4 – 10°E and 76 – 79°N) and calculating the correlation of the relative vorticity in the masked locations with the corresponding chlorophyll concentrations (denoted R^+). This calculation is then repeated for the absolute values of negative relative vorticity (R^-). A higher value of R thus indicates that high chlorophyll concentrations are connected to stronger rotation; R^+ shows the connection to cyclonic motion, R^- to anti-cyclonic motion. The resulting time varying correlations are plotted in Figure 5 along with the mean vertically integrated chlorophyll concentration in the whole area.

The modeled spring bloom starts in early May, and reaches its peak around the 1st of June, after which it begins to drop off again (Figure 5). The spring bloom thus coincides with Regime I, in which positive vorticity dominates productivity (Figure 5). Using the maximum gradient method (Method 5, Zawada et al., 2005), the mixed layer (ML) is defined as the depth where the density difference with respect to the surface equals 0.01 kg m^{-3} . The ML is shallowing during Regime I, while the DIN concentration at 20 m decreases during

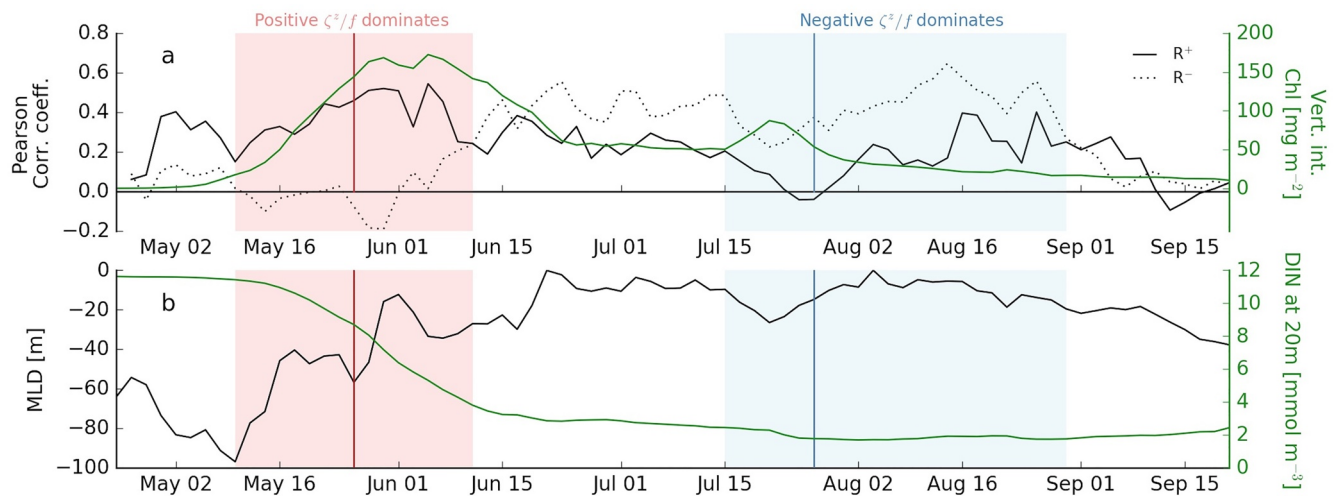


Figure 5. (a) Left axis: Correlation between vertically integrated chlorophyll and vorticity in water masses with vorticity values larger than 0.1 and smaller than -0.1 , respectively. Calculated for every second day from early May to late September. R^+ shows the connection to cyclonic motion, R^- to anti-cyclonic motion. Right axis: The average of the vertically integrated chlorophyll concentration calculated for every two days. The light pink box marks the time period in which the maximum chlorophyll concentration continuously is located in positive vorticity bins, and the blue box marks the time period in which the maximum chlorophyll concentration continuously is located in negative vorticity bins (see Figure 5). The pink and blue vertical lines mark the days which we look further into in the following figures. (b) Left axis: Mean mixed layer depth (MLD). Right axis: Mean dissolved inorganic nitrogen (DIN) concentration at 20 m.

the same period (Figure 5b), indicating a shift from light to nutrient limitation. R^+ is positive during Regime I, ranging from 0.2 to 0.5, with an average value of 0.38 ± 0.11 . The peak of the spring bloom coincides with the highest values of R^+ . The R^- values, are close to zero (-0.01 ± 0.1) during Regime I, but starting from the 1st of June, the value is positive, and increases over the following days. On the last day of Regime I, R^- becomes larger than R^+ (Figure 5a), thereby starting the intermediate period in which the chlorophyll concentration is elevated in both positive and negative filaments of vorticity (Figure 4). During the intermediate period, R^- has an average value of 0.43 ± 0.06 , and is thus consistently higher than the average R^+ value of 0.26 ± 0.06 . Regime II, characterized by the highest chlorophyll concentrations being located in the negative vorticity bins on average, occurs from mid-July to late August (Figure 4). During this time, the ML is relatively shallow and the DIN concentration at 20 m is low (Figure 5b), indicating a nutrient limited regime. During Regime II, the mean R^- -value is still 0.43 ± 0.11 , while R^+ has dropped to an R^+ -value of 0.17 ± 0.12 on average. The shift toward negative vorticity is thus brought on by a change in the correlation to the positive vorticity rather than a change in the correlation to negative vorticity.

3.4. Temporal Shift in Biological Drivers

During Regime I, from early May to mid-June, the MLD anomaly shows a clear pattern of a deeper ML in negative vorticity bins and shallower in positive bins (Figure 6a). The ML is thus shallower in positive vorticity bins in mid-May as compared to negative vorticity bins (Figure 5b), reducing light limitation here earlier in the season and explaining why the maximum chlorophyll anomaly is found in positive vorticity bins during Regime I (Figure 4). At the end of Regime I, in late June, the ML stabilizes in the whole WSC-area, with marginally deeper ML in areas close to zero, as illustrated by the negative anomaly (Figure 6a).

The average DIN concentration is similar across the vorticity bins until mid-May (Figure 6b). At this time, algae growth starts to reduce the surface DIN concentration (Figure 5b). This decrease is most marked in the positive vorticity bins as illustrated by the large dipole in the DIN anomaly between positive and negative vorticity bins (Figure 6b). Despite of a shift in the maximum chlorophyll to negative vorticity bins from mid-June onwards, the negative vorticity bins keep having a positive DIN anomaly for the remainder of the summer (Figure 6b). This positive and strong DIN anomaly can to some degree be explained by the positive vertical velocity here, leading to a positive anomaly in the vertical DIN flux (Figure 6c). An explanation for the shift to higher chlorophyll concentrations in negative vorticity bins during Regime II (Figure 4) is thus alleviation of nutrient limitation by vertical transport of DIN.

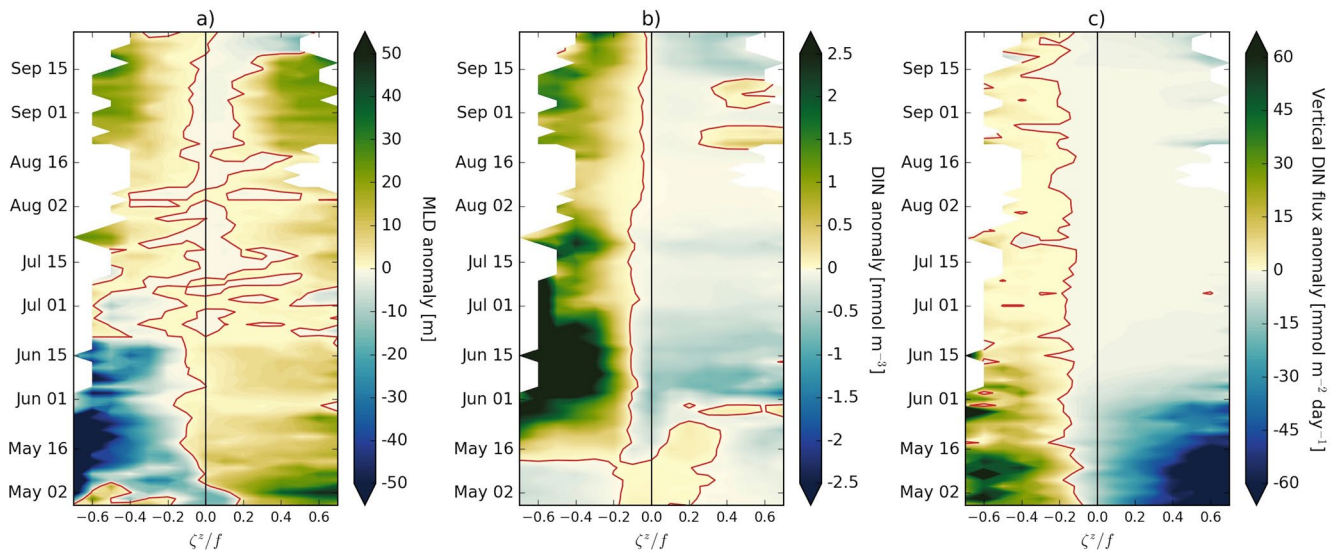


Figure 6. Daily anomalies of (a) the mixed layer depth calculated in vorticity bins of width 0.1. Here, positive anomalies indicate a shallower mixed layer (ML). (b) Dissolved inorganic nitrogen (DIN) concentration at 20 m depth calculated in vorticity bins of width 0.1 (c) the vertical DIN flux (vertical velocity times DIN concentration) at 20 m depth. All are calculated from early May to mid-September, with values for every second day. Calculations are carried out in the West Spitzbergen Current (WSC) ($4 - 10^\circ\text{E}$ and $76 - 79^\circ\text{N}$).

3.5. Role of Eddies Versus Filaments

During Regime II, the highest chlorophyll concentrations were associated with negative vorticity, but elevated chlorophyll also occurred in positive vorticity bins (Figures 4 and 5). This cannot be explained with nutrient upwelling in closed-core eddies, so we investigate also the relative role of filaments versus eddies.

To identify the location of eddies, we use the Okubo-Weiss method (Equation 1). For vorticity bins with $|\zeta^2/f| > 0.1$, we separate the surface into areas of cyclonic and anti-cyclonic eddies (characterized by a core of positive and negative vorticity, respectively), positive vorticity filaments, and negative vorticity filaments. As the vorticity bins with values close to zero tend to be distinct with respect to bins of stronger vorticity, areas with $|\zeta^2/f| < 0.1$ have been pooled into one category. For each of these categories, we have calculated timeseries of anomalies by subtracting the average of the whole WSC area from the average within each category (Figure 7). The percentage of the total area falling within each category has been plotted in Figure A2, illustrating that the areas of $|\zeta^2/f| > 0.1$ decrease in mid-August, as the general eddy strength decreases.

Early in Regime I, the chlorophyll anomaly is positive in both cyclonic eddies and positive vorticity filaments (Figure 7a) at the same time as the ML anomaly is positive (Figure 7b). However, from late May, when the bloom reaches its' peak (Figure 5a), the chlorophyll anomaly decreases in the cyclonic eddies, becomes negative at the end of Regime I, and stays close to zero for the rest of the summer (Figure 7a). The decrease in chlorophyll anomaly in the cyclonic eddies coincides with a decrease in the DIN anomaly (Figure 7b). Cyclonic eddies thus mainly play a role before the peak of the spring bloom, when they are characterized by a shallow ML and before the available DIN has been depleted. While the chlorophyll anomaly of the cyclonic eddies decreases in late May, the anomaly of the positive vorticity filaments stays high until late June, at which time it decreases but stays positive for the remainder of the summer (Figure 7a). The sustained high chlorophyll concentration in positive vorticity bins in the late part of Regime I and onwards (Figure 4) is thus brought on by growth in the positive vorticity filaments. This is consistent with DIN anomalies being consistently higher in the positive vorticity filaments than in the cyclonic eddies (Figure 7c). The simultaneous decrease in the chlorophyll and DIN-flux anomaly, and the convergence of ML-anomalies toward zero in mid-June (Figures 7b and 7d), however, suggests that the decrease in the chlorophyll anomaly is brought on by a less dynamic water column and thus a smaller supply of nutrients, which in turn is affected by the general drawdown of DIN (Figure 7c).

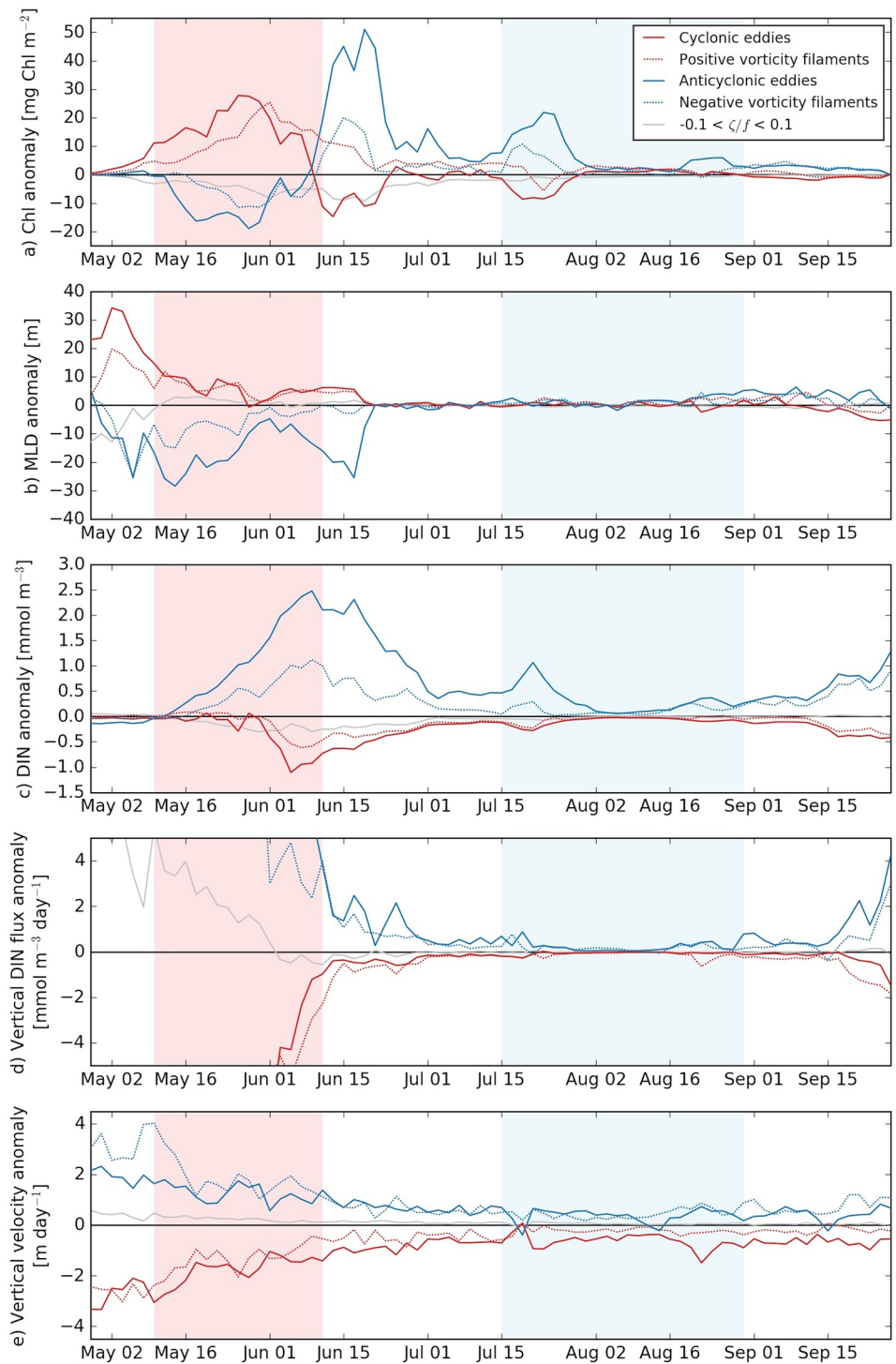


Figure 7. Daily anomalies separated into cyclonic and anticyclonic eddies, filaments of positive and negative vorticity, and areas with $|\zeta/f| < 0.1$: (a) Chlorophyll concentration, (b) Mixed layer depth, (c) dissolved inorganic nitrogen (DIN) concentration, (d) Upwelling of DIN at 20 m, (e) Vertical velocity. The pink and blue backgrounds mark Regime I and II, respectively.

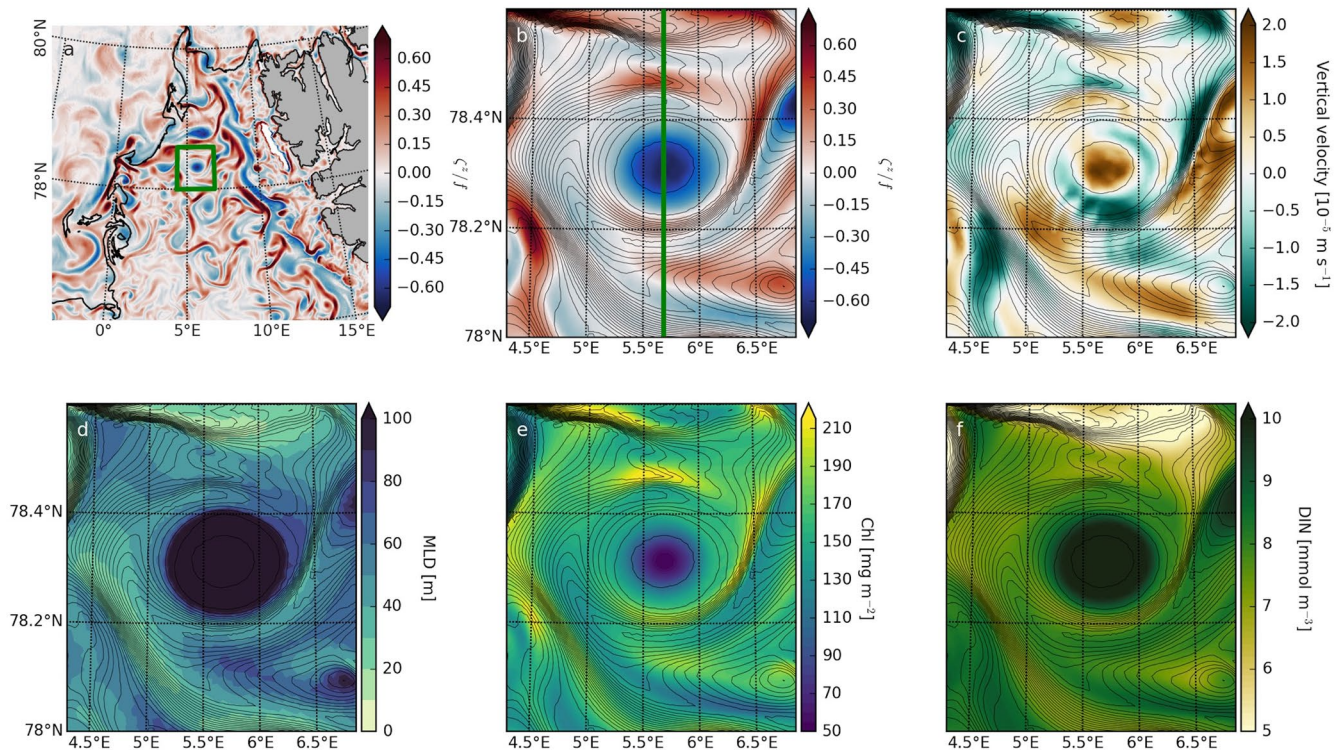


Figure 8. Close-up of an anticyclonic eddy in the WSC during Regime I on the 27th of May. (a) Fram Strait spatial distribution of relative vorticity normalized by f in the surface water on the 27th of May. The green square marks the location of the eddy shown in subplot (b–f). The black line marks the 10% ice concentration contour. (b) Surface relative vorticity normalized by f . (c) Vertical velocity at 40 m, approximately the depth of the mixed layer base. (d) Depth of the mixed layer, based on a density difference of 0.01 kg m^{-3} with respect to the surface. (e) Vertically integrated chlorophyll concentration. (f) Surface dissolved inorganic nitrogen (DIN) concentration. The black lines are isopycnals with a distance of 0.004 kg m^{-3} . The green line marks the location of the section in Figure 9.

For the negative vorticity, the signal of the eddies and filaments follows the same pattern regarding the chlorophyll and DIN anomaly throughout the summer, though the signal of the eddies is consistently stronger (Figures 7a and 7c). During Regime I, deep ML causes the chlorophyll anomaly of the anti-cyclonic eddies to be negative, while the DIN anomaly is strong and positive. Notice that the depth across which the vertical DIN transport is calculated (20 m) is above the base of the mixed layer in the negative vorticity areas early in summer before the water column is stabilized. As the chlorophyll anomaly switches to strongly positive at the end of Regime I, the DIN anomaly decreases as DIN is drawn down (Figure 7c). At this time, the water column has stabilized with shallower mixed layer across the vorticity bins.

3.6. Regime I: Chlorophyll Associated With Positive Vorticity

To further illustrate the mechanisms driving biological productivity during Regime I (Figure 5), we now look in detail at an anticyclonic eddy located in the WSC (5.7°E and 78.3°N , Figure 8a). We focus on the 27th of May, well after the initiation of the spring bloom, just before the bloom peaks (Figure 5).

This anticyclonic eddy has a diameter of $\sim 30 \text{ km}$, with a clear center of negative vorticity, surrounded by filaments of positive and negative vorticity (Figures 8b and 9a). The relative vorticity normalized by f has values between -0.7 and 0.7 in the area, with the strongest vorticity at the surface (Figure 9b). The core of the eddy is surrounded by a clockwise flow (Figure A3), as can also be inferred from the horizontal stretching of the isopycnals (Figure 8). The horizontal velocity reaches values higher than 0.3 m s^{-1} in the flow surrounding the eddy (Figure A3). This speed appears to be a realistic increase of the typical maximum of 0.1 m s^{-1} reported by von Appen et al. (2016). The center of the eddy is characterized by upwelling, as is also the tendency in the surrounding filaments of negative vorticity (Figure 8c). The upwelling in the center of the eddy leads to divergence at the surface, while downwelling in and convergence toward the positive

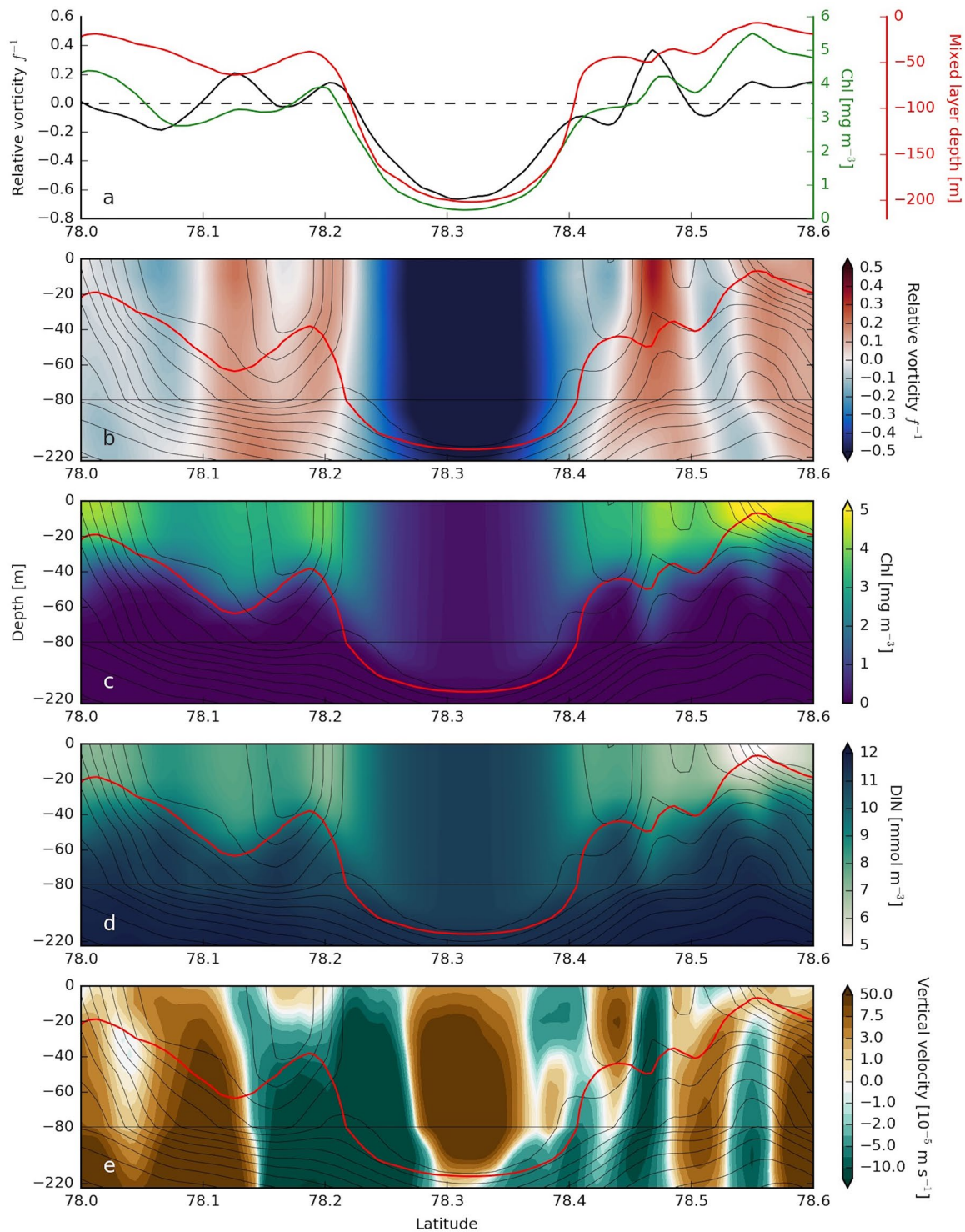


Figure 9. May 27th. North-south section through the Regime I anticyclonic eddy (Figure 8) at 5.7°E (Figure 8b). (a) Surface values of relative vorticity, chlorophyll concentration and mixed layer depth along the section. The dashed black line marks 0 vorticity. (b) Relative vorticity normalized by f . (c) Chlorophyll concentration. (d) dissolved inorganic nitrogen (DIN) concentration. (e) Vertical velocity. The black lines are isopycnals with a distance of 0.01 kg m⁻³. Notice the nonlinear y-axis.

vorticity filaments leads to compression of the isopycnals (Figure 8). In the vertical, the isopycnals are sloping downwards in the core of the eddy, leading to weak stratification with some instability (Figure 9). The ML ranges from 200 m in the center of the eddy, to 10–40 in the surrounding water (Figures 8d and 9). It appears to be especially shallow in areas where the isopycnals are horizontally compressed (Figure 8d and 9), and thus also in areas of positive vorticity (Figure 8b), as illustrated in Figure 6a.

The chlorophyll concentration tends toward elevated values in the positive vorticity filaments (Figures 8b, 8e and 9a), consistent with the positive correlation between positive vorticity and chlorophyll during Regime I (Figure 5). Additionally, the positive vorticity filaments and high chlorophyll concentrations coincide with areas of shallow ML, both in the horizontal (Figures 8b, 8d, and 8e) and the vertical domain (Figures 9a and 9c). In the vertical, the elevated chlorophyll concentrations only appear below the ML, where the chlorophyll is subject to vertical transport by downwelling (Figures 9b and 9d). This connection between chlorophyll and the depth of the ML supports the statement that light limitation plays a significant role in controlling productivity at this time. The role of light is further confirmed by the fact that the DIN concentration is higher than 5 mmol m^{-3} in the surface water surrounding the eddy (Figures 8f, 9a, and 9c) and thus too high to be limiting production. Additionally, the high chlorophyll concentrations coincide with areas of low DIN concentrations, showing that DIN has been drawn down to a higher degree where productivity occurs, but not to the extent that it is limiting. While the dynamics of the eddy does not appear to directly impact productivity by supplying DIN to the surface water, the upwelling in the core of the eddy pumps the DIN from below the nutricline into the ML, where divergence acts to move it away from the center, thereby indirectly resupplying the surface DIN concentration further away from the eddy center.

In Figure 8, areas of high chlorophyll concentration and shallow ML coincide with horizontally compressed isopycnals, suggesting that horizontal transport further acts to increase the surface chlorophyll concentration in areas of convergence.

To summarize, the elevated chlorophyll concentration in the positive vorticity filaments is caused a shallow ML, leading to less light limitation, and possibly also horizontal transport through convergence of water masses.

3.7. Regime II: Chlorophyll More Associated With Negative Than Positive Vorticity

To illustrate the tendency of higher chlorophyll concentrations in negative vorticity filaments and eddies from mid-July to late August (Figure 5), we focus on an anti-cyclonic eddy located at 8.8°E and 78.3°N (Figure 10a). This is the same latitude as the anti-cyclonic eddy in Figure 8, but further to the east. The diameter of this eddy is likewise ~ 30 km. We look at the 27th of July, 2 months later than the day of the Regime I eddy (Figure 5). At this time, the average chlorophyll concentration in the WSC has fallen significantly, as compared to the maximum in early June, but is still high enough for productivity to be widespread across Fram Strait. Had we chosen a later date, the productivity would be lower and more local. The 27th of July falls just after a wind event, which has led to increased chlorophyll concentration in the area during the preceding days (Figure 5).

Compared to the eddy in Regime I (Figure 8), the relative vorticity normalized by f is now weaker, ranging from -0.2 to 0.5 in the area plotted (Figure 10b), in line with vorticity observations from Fram Strait (von Appen et al., 2016). The weaker relative vorticity in turn leads to less strong horizontal density gradients and a less filamented distribution around the eddy compared to the eddy in May (Figures 8b and 10b). The eddy has a well-defined center, characterized by low vorticity values, and is surrounded by a clockwise flow. The current surrounding the eddy has a strength of $\sim 0.2 \text{ m s}^{-1}$ (Figure A4). Toward the west, the horizontal flow is dominated by a strong northward flowing filament of the WSC, skirting the edge of the eddy (Figure A4). The depth of the ML is generally shallower (~ 10 – 40 m) and the stratification stronger than the situation in May (Figure 10d).

In the center of the eddy, the isopycnals are displaced upwards close to the surface, and downwards deeper in the water column (Figure 11), effectively trapping the weakly stratified water mass in between. The eddy is thus a so-called mode water eddy (McWilliams, 1985), which have been shown to act as retention centers for biological productivity (d'Ovidio et al., 2013). The highest chlorophyll concentrations are located in the center of the eddy, especially in the south-eastern part (Figures 10e and 11c), where the isopycnals

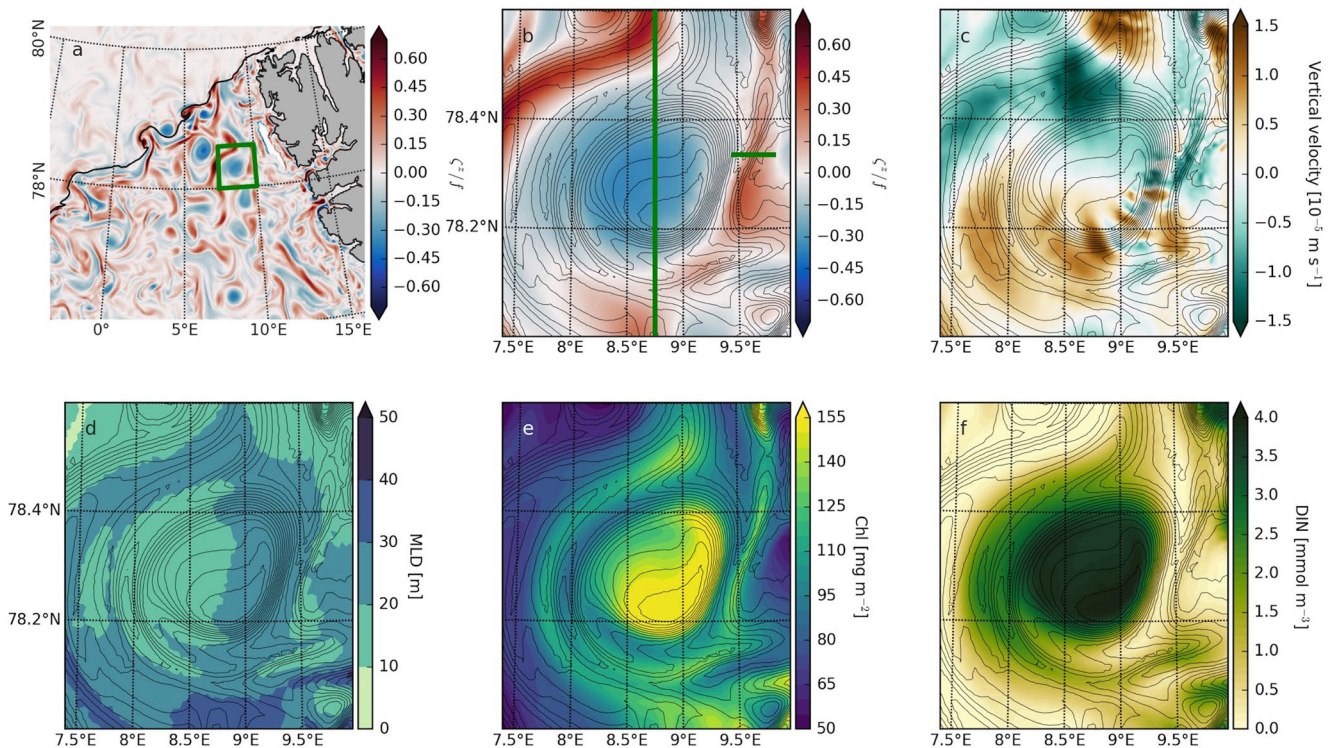


Figure 10. Close-up of an anticyclonic eddy in the West Spitzbergen Current (WSC) during Regime II on July 27th. (a) Fram Strait spatial distribution of relative vorticity normalized by f in the surface water on the 27th of May. The green square marks the location of the eddy shown in subplot (b–f). The black line marks the 10% ice-concentration contour. (b) Surface relative vorticity normalized by f . (c) Vertical velocity at 40 m, approximately the depth of the mixed layer base. (d) Depth of the mixed layer, based on a density difference of 0.01 kg m^{-3} with respect to the surface. (e) Vertically integrated chlorophyll concentration. (f) Surface dissolved inorganic nitrogen (DIN) concentration. The black lines are isopycnals with a distance of 0.004 kg m^{-3} . The green lines mark the location of the sections in Figure 11.

and the surface DIN concentration is elevated (Figure 10f). The eddy is characterized by upwelling in the south-western part of the eddy and downwelling in the north-eastern part (Figure 10c). In much of the surrounding water, the DIN concentration is low enough to be limiting. The higher DIN concentrations in the eddy center is likely brought on by the vertical DIN transport through upwelling (Figures 11a and 11g) combined with the doming isopycnals of the mode water eddy, bringing the nutricline upwards in the water column (Figures 11a and 11g), an effect that can also be observed in areas of increased chlorophyll north and south of the eddy (Figures 11a and 11e). In the eddy center, the isopycnals are more elevated than in the surrounding water, and the high chlorophyll concentration is limited to the upper 20 m of the water column (Figures 11c and 11d). In the surrounding filaments, the isopycnals are not doming to the same degree, meaning that the chlorophyll concentration is lower (Figure 11a), but distributed over a larger depth span; down to 40 m south of the eddy and down to 60 m north of the eddy, leading to the relatively high values of vertically integrated chlorophyll concentrations in Figure 10e. It is thus likely that some degree of light limitation through self-shading is taking place in the eddy center. Overall, however, this distribution of the chlorophyll and DIN points to nutrient limitation playing a larger role than what was the case during Regime I.

As predicted in Figure 4, the chlorophyll is also elevated in some of the positive vorticity filaments surrounding the eddy. One example is the filament of high chlorophyll on the east side of the core (Figure 10e). This filament is located at the frontal zone between northward flowing water to the east and southward flowing to the west (Figure A4c), with upwelling along the frontal zone (Figure 10j). As was the case in filaments of positive vorticity in Regime I, the horizontal isopycnals are compressed in the frontal area due to convergence and resulting downwelling (Figure 11j). This convergence may bring in nutrients from the upwelled water at the edges of the front. However, in cyclonic eddies, isopycnals are generally doming upwards in the positive vorticity core (e.g., McGillicuddy, 2016) and this tendency is also seen in this positive vorticity filament (Figure 11j). The raised pycnocline coincides with the maximum chlorophyll

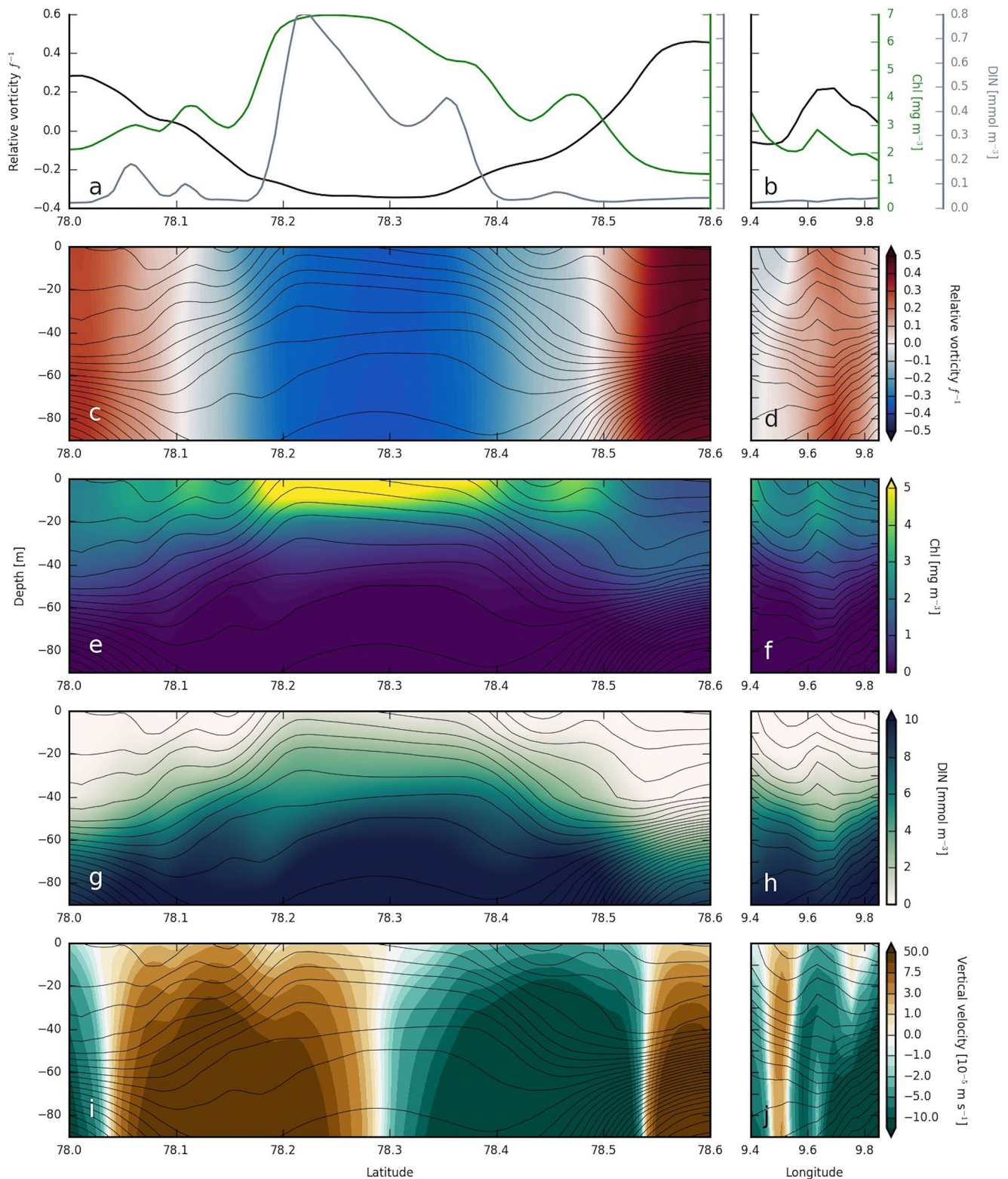


Figure 11. July 27th. Left column: North-south section through the anti-cyclonic eddy of Regime II (Figure 8) at 8.7°E. The section is marked in Figure 10b. Right column: East-West section through positive vorticity filament at 78.35°N. The filament is located east of the Regime II anti-cyclonic eddy, along 9.6°E (Figure 10b). (a and b) Surface values of relative vorticity, chlorophyll concentration and DIN along the section. (c and d) Relative vorticity normalized by f . (e and f) Chlorophyll concentration. (g and h) DIN concentration. (i and j) Vertical velocity, positive values are upwards. The black lines are isopycnals with a distance of 0.01 kg m⁻³.

concentration (Figure 10e) and may thus act to bring up the nutricline to induce algae growth. While the surface DIN concentration is not elevated (Figures 11a and 11h), it is possible that this is a consequence of biological drawdown in the surface.

A third feature in the surroundings of the eddy is the elevated chlorophyll west of the core (Figure 10e). This is not a frontal zone, or a zone of high vorticity, but rather colocated with the stronger main current of the WSC (Figure A4c). The most likely explanation for the elevated DIN and chlorophyll concentrations here is vertical and the horizontal shear.

The distribution of chlorophyll, isopycnals and the nutrient concentration show that the bloom at this stage is more nutrient limited than what was the case 2 months earlier. Chlorophyll and DIN concentrations are elevated in areas of both negative and positive vorticity, though stronger in the negative vorticity regions. In the region plotted (Figure 10), a common feature is the upwards doming of the isopycnals, which brings nutrients toward the surface and thus may sustain phytoplankton growth.

4. Discussion

4.1. Light Control of Chlorophyll Enhancement

In accordance with the critical depth hypothesis by Sverdrup (1953), the spring bloom in the open waters of eastern Fram Strait is thought to be initiated when surface heat fluxes act to stratify the water column during the month of May (Cherkasheva et al., 2014; Randelhoff et al., 2018). Our study supports this theory, and suggests that stratification plays a driving role in the period from bloom onset in early May to the bloom decreases in early June (Figure 5). Further, we show that the eddy field introduces a large degree of spatial heterogeneity in this stabilization on a scale of several kilometers, as areas of positive relative vorticity are stratified earlier than areas of negative relative vorticity (Figures 6–8). Similar mesoscale effects have been shown to affect the spring bloom south of Iceland (Mahadevan et al., 2012). In a combined satellite and model study of the Southern Ocean, Song et al. (2018) showed that cyclonic eddies were characterized by a shallow ML relative to anticyclonic eddies. While their study covered a wider meridional range ($\text{lat} < -40^\circ$), with an associated longer growth season, their findings of chlorophyll enhancement in cyclonic eddies in times of light limitation is consistent with our results. In the Labrador Sea, eddies are thought to contribute to shoaling and restratification of the mixed layer (Chanut et al., 2008), while a large degree of heterogeneity has been observed in the early bloom of Baffin Bay (Frajka-Williams et al., 2009). In the latter study, the eddies are generated along the east coast of Greenland, thus introducing stratification by transporting cold meltwater toward the open water of Baffin Bay. Similarly, starting in May, filamented patches of cold and fresh melt water are carried northward from the southern tip of Spitzbergen in our simulation, thus likely contributing to the mixed layer shoaling in the WSC we observe (Figure 8d). Another factor that affects the degree of stratification in Fram Strait, is cold water from the melting ice edge (Cherkasheva et al., 2014; Lester et al., 2020). In our model run, the early bloom does, in fact, start in the ice zone (not shown), but whether tongues of melt water are able to move in the south-westerly direction, against the general direction of the current and pathway of the eddies, is an open question.

The tendency of patches of shallow ML and high chlorophyll concentration correlating with positive vorticity areas (Figures 4 and 5) has been previously observed (e.g., Dufois et al., 2014; Kouketsu et al., 2011). Further, in a study from the Sea of Japan, satellite-based observations have shown that the spring bloom is delayed in the center of anticyclonic eddies where the ML was relatively deep, while the positive vorticity edges of the eddies were stratified to a shallower depth and thus had an earlier bloom (Maure et al., 2017).

4.2. Horizontal Convergence and Chlorophyll

Elevated chlorophyll concentrations in May and June coincide with areas of horizontally compressed isopycnals (Figure 8), suggesting that the mechanism behind increased chlorophyll concentration is two-fold: alleviation of light limitation through ML shallowing and up-concentration due to horizontal convergence. Several studies have used Lagrangian methods to show that mesoscale dynamics can trap phytoplankton in convergent filaments of convergence. Here the convergent horizontal nutrient advection can create a physical niche that lasts long enough for a bloom to develop (d'Ovidio et al., 2010; Lehahn et al., 2007),

provided that the rate of phytoplankton growth here is higher than the rate of subduction. In the Norwegian Sea, Samuelsen et al. (2012) showed that particles released in an anticyclonic eddy end up at the edge of the eddy, similar to the imprint we see in May and June (Figure 8), before the entire area is stratified. Additionally, zooplankton and mesopelagic fish have been shown to feed along the edges of anticyclonic eddies (Godø et al., 2012), further indicating that phytoplankton, on which they prey, is located here.

The submesoscale field of the surface ocean changes over time, with developing eddies and filaments. Phytoplankton trapped in a water parcel will also be distorted by the changing shape of the filament as was also observed by d'Ovidio et al. (2010). An example is the positive vorticity filament in Figure 10. Our results show a clear connection between positive vorticity and chlorophyll concentration in May and June (Figures 4 and 5), but upon closer inspection, concentrations are also elevated downstream of these hot-spots (Figure 8). This deformation of the bloom, which occurs in three-dimensional space, makes it more difficult to obtain straight-forward answers about the processes driving the productivity, as stirring of the field means that the phytoplankton is transported with the current to areas with some degree of different properties (e.g., Abraham et al., 2000).

4.3. Chlorophyll Enhancement by Nutrient Modulation

In the period from mid-July to late August (Regime II), the highest chlorophyll concentrations are found in areas of negative vorticity in our study (Figure 4). During this period, the surface water DIN concentration is low enough to be limiting (Figure 10). However, at 20 m, the DIN concentration and the vertical transport of DIN is elevated in negative vorticity areas (Figures 6b and 6c), thus partly explaining the sustained productivity here. Similar nutrient enhancement in negative vorticity areas (anti-cyclonic eddies) has been observed during the nutrient limited Southern Ocean summer (Song et al., 2018), explained by the month-long lifetime of the eddies, and thus connection to the preconditioning during winter. In Fram Strait, however, the lifetime of the eddies are on the order of 10 days (Wekerle et al., 2020), suggesting that other mechanisms are at play here. Studies from the North Atlantic Ocean have suggested that ageostrophic circulation within the eddy rather than wind-driven Ekman pumping (Martin & Richards, 2001) was the mechanism behind high chlorophyll anomalies in the surface water of the eddy (Ledwell et al., 2008), while Rohr et al. (2020) showed that wind driven Ekman-pumping is driving vertical nutrient supply to the anti-cyclonic eddies in the Southern Ocean. From our results, the role of the vertical velocity, however, remains unclear; the upwelling seen in negative vorticity regions (Figure 6) may be less prominent than it appears as it is partly induced by the propagation of eddies and front. Additionally, the nutrient upwelling and the doming and suppression of the pycnocline are both driven by the vertical velocity.

We have illustrated Regime II with a mode-water eddy in Fram Strait (Figure 11), generally characterized by upwards deflection of isopycnals, and thus the nutricline (e.g., McGillicuddy et al., 1999). In a nutrient limited regime, this doming of the nutricline will act to support productivity like we see in Fram Strait (Figure 11c). The surface vorticity distribution of mode-water eddies is similar to the one of anticyclonic eddies, while the sea surface height signature is similar to the one of cyclonic eddies, making it difficult to determine the relative number of normal versus mode-water anticyclonic eddies. However, the relative vorticity of strong eddies is connected to the water masses of which they are composed; early in the season, the WSC is a strong jet with positive relative vorticity on its seaward side and negative relative vorticity on the side of Svalbard. It is unstable, and breaks into the pattern seen in Figure 2. Strong anticyclones are formed in the area, containing warm water of Atlantic origin (Figure 2b). In late summer, melt water has stratified the surface water (Figure 5b), generating mode water eddies with a shallow stable stratification at the top. The seasonal changes in water mass properties suggest that the WSC is indeed dominated by anticyclonic mode-water eddies with doming isopycnals, and it is thus plausible that the increased chlorophyll anomaly in negative vorticity areas is caused by raised nutriclines as suggested in Figure 11, as well as upwelling (Figure 6).

The semi-closed cores of anticyclonic mode-water eddies are able to transport properties, and thus nutrients, across large distances (e.g., von Appen et al., 2020; Xu et al., 2017), with the nature of transported properties depending on the water masses in the area where the eddy originated. Only few eddies are generated on the Svalbard shelf in our simulation, while more originate in eastern Fram Strait and move in the north-westwards direction (Wekerle et al., 2020). Considering that the water in the WSC is relatively rich in

nutrients (Torres-Valdés et al., 2013) it is possible that one reason for the high chlorophyll concentration in areas of negative vorticity (Figure 4) is trapping and transport of nutrients.

The sustained high chlorophyll concentrations in bins of positive vorticity (Figure 4) are driven by relatively high chlorophyll anomalies within cyclonic filaments rather than eddies (Figure 7). A common feature of positive vorticity filaments, cyclonic eddies and mode-water eddies is the doming isopycnals (Figure 11). This doming may account for some of the signal, however, the lack of high anomalies within cyclonic eddies suggests that other factors are at play. We speculate that nutrient trapping within the cyclonic eddies indeed plays a role; cyclonic eddies can be seen as semi-closed entities with limited exchange of properties with surrounding water. Productivity within cyclonic eddies are thus to a larger degree dependent on preconditioning with nutrient-rich water than what is the case for cyclonic filaments in which lateral transport may play a larger role.

Fadeev et al. (2021) showed that the biological activity was elevated in a filament of positive vorticity in the marginal ice zone of Fram Strait. This study was carried out on the 29th of July, thus effectively coinciding with the day we have focused on for Regime II (the 27th of July, Figure 5). This filament was characterized by convergence, downwelling and upwards sloping isopycnals. The same characteristics are seen in the section of a positive vorticity filament in our study (Figure 11). In the Chuckchi Sea, Nishino et al. (2018) found elevated chlorophyll within a nutrient limited cyclonic eddy, they attributed this to raised isopycnals and double-diffusive mixing processes. This indicates that the lack of chlorophyll in cyclonic eddies later in the season in our study is indeed due to the depleted eddy inventory of nutrients combined with an absence of lateral nutrient transport.

4.4. Advantages and Limitations of the Model

In our model setup, the horizontal resolution in Fram Strait equals 1 km, smaller than the Rossby Radius in the area (4–6 km, von Appen et al., 2016), making it possible to resolve mesoscale dynamics. FESOM does a good job in representing the mesoscale dynamics in this setup, including eddy driven return flow, life time of eddies and strength of vorticity (Wekerle, Wang, von Appen, et al., 2017; Wekerle et al., 2020), nevertheless, processes on a smaller scale than ~2 km are not captured. These submesoscale processes are increasingly thought to play an important role for marine ecosystems (Mahadevan, 2016), affecting processes such as transient upwelling of nutrients (Brannigan, 2016; Uchida et al., 2020) and restratification of the surface mixed layer in spring (Brody et al., 2016). Despite of the multi-resolution setup of FESOM, the simulation shown here is computationally challenging, especially as the biogeochemical module adds 21 tracers, and at this stage, we are not able to capture submesoscale processes as mentioned above.

A strength of our setup is that we have a relatively realistic model run, including seasonal changes such as ice melting and formation, changes in the circulation pattern, the intensity of incoming light and a realistic geometry. Additionally, the simulation includes episodic occurrences, such as wind events, adding to the complexity. In short, the model run is attempting to mimic the world as it is as opposed to an idealized setup. The drawback is that such a model run is relatively complicated to analyze and does not give direct connections between controlled processes as in idealized model runs that focus on a specific process (e.g., Levy & Klein, 2004; Ramachandran et al., 2014).

5. Conclusions

In general, the connection between the physical dynamics of eddies and biology is complicated, due to the complexity and nonsteady state of both the eddy field and the biology. Whether cyclonic or anti-cyclonic eddies act to drive or suppress production in Fram Strait, depends on, for example, time and place, how the eddy was formed and where it was formed.

Based on a high-resolution model run of sea ice, ocean, and biogeochemistry, we have shown that mesoscale dynamics of eddies and filaments have a strong imprint on the surface field of the biological properties, and act to shape the progression of the bloom during summer. The effect of the mesoscale variability on chlorophyll can be divided into two regimes; during Regime I, high chlorophyll concentrations are predominantly associated with high values of positive vorticity, while they are predominantly associated with

large values of negative vorticity during Regime II. Regime I takes place at the time of the spring bloom in May and June. At this time, high chlorophyll concentration mainly occurs in areas of shoaling mixed layers and converging water masses, indicating that light and up-concentration of the biomass plays a role at this stage, while nutrients are not limiting. Regime II starts in mid-July, when the maximum chlorophyll values are associated with negative vorticity values. At this time, nutrient limitation is important for control of phytoplankton growth, as the mixed layer is well defined and shallower, and surface DIN concentrations are low. Upwelling of nutrients occur in negative vorticity areas, acting to sustain productivity here, though upward-sloping isopycnals may also play a role. During Regime II, the chlorophyll concentration is likewise to some degree elevated in filaments of positive vorticity, pointing toward importance of lateral nutrient transport.

In Fram Strait, the mesoscale eddy field modulates the upper ocean in ways that can be conducive for or suppressing phytoplankton growth, depending on the circumstances. In the current study, we take a first step with a global biogeochemical model toward explaining this complex mesoscale interplay between physics and biology. Considering the effort that is put into monitoring this main gateway to the Arctic Ocean, a better understanding of mesoscale effects on the system will improve our interpretation of the observations.

Appendix A: Supporting Figures

A1. Distribution of Vorticity

The study site is characterized by most of the area falling within bins of low vorticity strength from May to October. As the vorticity field weakens over the summer, this tendency becomes stronger (Figure A1).

Dividing the study area into anti-cyclonic eddies, anti-cyclonic filaments, cyclonic eddies and cyclonic filaments, these areas make up between 6 and 10% of the study area in early May, with a decreasing trend over time due to a decrease in the vorticity strength (Figure A2).

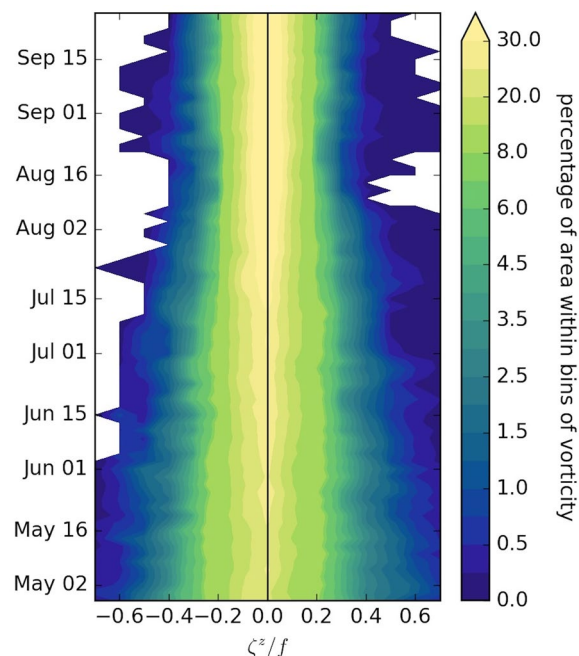


Figure A1. Percentage area within bins of vorticity used for Figures 4 and 6. Notice the nonlinear color scale.

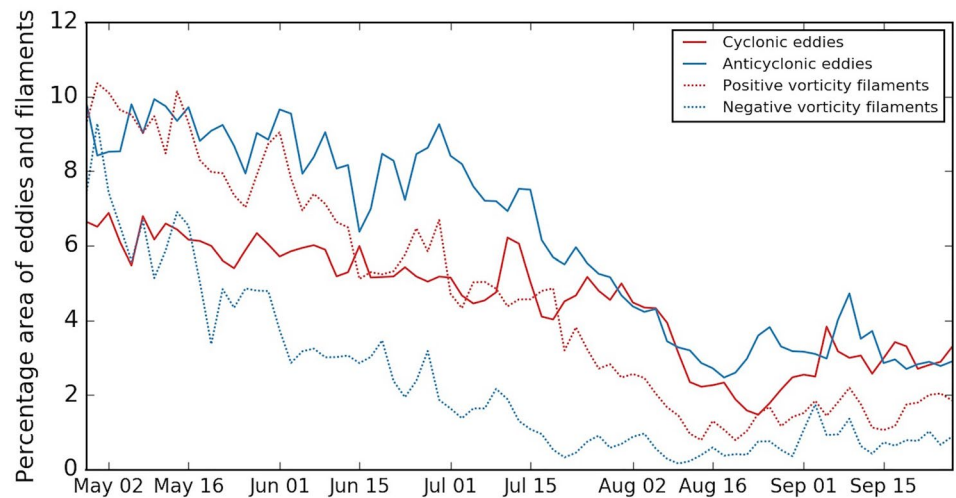


Figure A2. Development of the percentage area located within cyclonic and anticyclonic eddies and in positive and negative vorticity filaments. The eddies have been detected using the Okubo-Weiss algorithm (Equation 1), and only areas where $|\zeta / f| > 0.1$ are included.

A2. Surface Velocity

The anti-cyclonic eddy plotted for the 27th of May is encircled by a clock-wise flow, and surrounded by smaller eddies and filaments, which likewise show local intensification of the current speed (Figure A3).

On July 27th, the strength of the eddy field has weakened, leading to a weaker flow surrounding an anti-cyclonic eddy on this day (Figure A4).

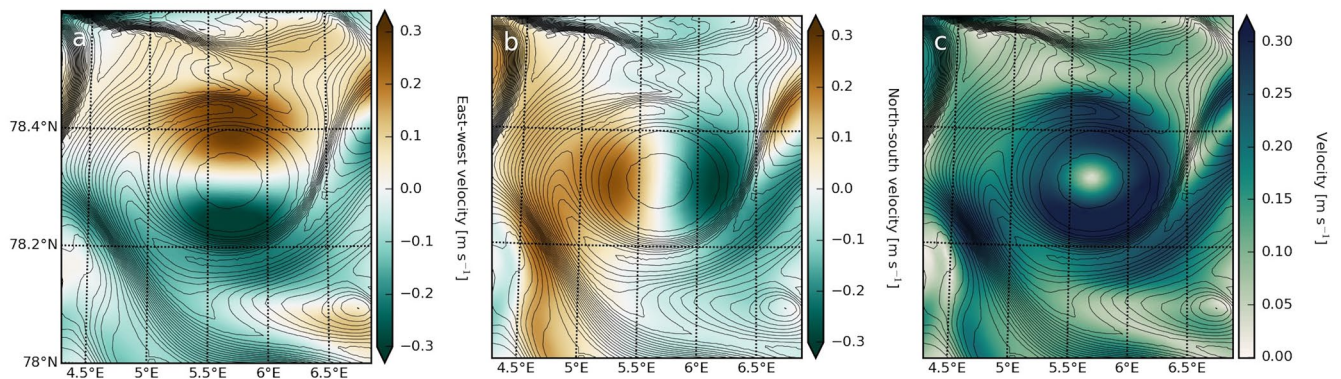


Figure A3. Zoom of an anticyclonic eddy in the WSC on May 27th, during the positive vorticity chlorophyll regime. (a) East-west component of velocity (u). (b) North-south component of velocity (v). (c) Absolute velocity $vel = (u^2 + v^2)^{0.5}$.

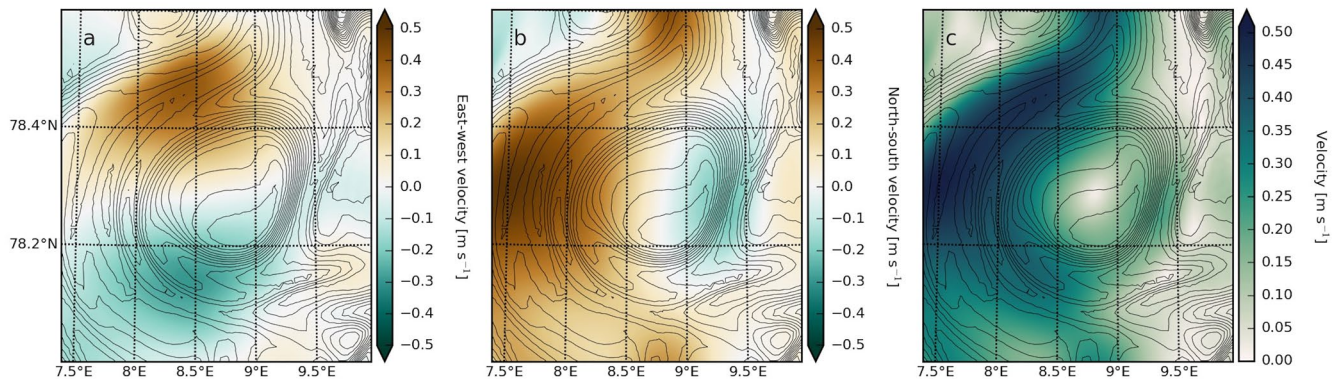


Figure A4. Zoom of an anticyclonic eddy in the WSC on July 27th, during the negative vorticity chlorophyll regime. (a) East-west component of velocity (u). (b) North-south component of velocity (v). (c) Absolute velocity $vel = (u^2 + v^2)^{-0.5}$.

Data Availability Statement

Computational resources were made available by the Norddeutscher Verbund für Hoch- und Höchstleistungsrechnen (HLRN). The biogeochemical model data from REcoM2 used in this study is available from <https://zenodo.org/record/4536806#.YCZzfBNKjOQ>. Please refer to Wekerle, Wang, von Appen, et al. (2017) for the physical model output from FESOM.

Acknowledgments

The authors would like to thank the FESOM team and FRAM community at the Alfred Wegener Institute for support and discussions regarding this study. V. Schourup-Kristensen and C. Wekerle were funded by the FRontiers in Arctic marine Monitoring program (FRAM). C. W was further supported by funds of the German Federal Ministry of Education and Research (BMBF), project Greenland Ice Sheet/Ocean Interaction (GROCE-2), grant no. 03F0855A. Open access funding enabled and organized by Projekt DEAL.

References

- Abraham, E. R., Law, C. S., Boyd, P. W., Lavender, S. J., Maldonado, M. T., & Bowie, A. R. (2000). Importance of stirring in the development of an iron-fertilized phytoplankton bloom. *Nature*, *407*(6805), 727–730. <https://doi.org/10.1038/35037555>
- Aumont, O., & Bopp, L. (2006). Globalizing results from ocean in situ iron fertilization studies. *Global Biogeochemical Cycles*, *20*, GB2017. <https://doi.org/10.1029/2005GB002591>
- Beszczynska-Moller, A., Fahrbach, E., Schauer, U., & Hansen, E. (2012). Variability in Atlantic water temperature and transport at the entrance to the Arctic Ocean, 1997–2010. *ICES Journal of Marine Science*, *69*(5), 852–863. <https://doi.org/10.1093/icesjms/fss056>
- Brannigan, L. (2016). Intense submesoscale upwelling in anticyclonic eddies. *Geophysical Research Letters*, *43*(7), 3360–3369. <https://doi.org/10.1002/2016GL067926>
- Brody, S. R., Lozier, M. S., & Mahadevan, A. (2016). Quantifying the impact of submesoscale processes on the spring phytoplankton bloom in a turbulent upper ocean using a Lagrangian approach. *Geophysical Research Letters*, *43*(10), 5160–5169. [https://doi.org/10.1002/\(ISSN\)1944-800710.1002/2016gl068051](https://doi.org/10.1002/(ISSN)1944-800710.1002/2016gl068051)
- Capet, X., McWilliams, J., Molemaker, M. J., & Shchepetkin, A. F. (2008). Mesoscale to submesoscale transition in the California Current System. Part I: Flow structure, eddy flux, and observational tests. *Journal of Physical Oceanography*, *38*(1), 29–43. <https://doi.org/10.1175/2007JPO3671.1>
- Carpenter, J., & Timmermans, M.-L. (2012). Deep mesoscale eddies in the Canada Basin, Arctic Ocean. *Geophysical Research Letters*, *39*(20). <https://doi.org/10.1029/2012GL053025>
- Chanut, J., Barnier, B., Large, W., Debreu, L., Penduff, T., Molines, J. M., & Mathiot, P. (2008). Mesoscale eddies in the Labrador Sea and their contribution to convection and restratification. *Journal of Physical Oceanography*, *38*(8), 1617–1643. <https://doi.org/10.1175/2008JPO3485.1>
- Chassignet, E. P., Yeager, S. G., Fox-Kemper, B., Bozec, A., Castruccio, F., Danabasoglu, G., et al. (2020). Impact of horizontal resolution on global ocean–sea ice model simulations based on the experimental protocols of the Ocean Model Intercomparison Project phase 2 (OMIP-2). *Geoscientific Model Development*, *13*(9), 4595–4637. <https://doi.org/10.5194/gmd-2019-37410.5194/gmd-13-4595-2020>
- Chen, C., Gao, G., Zhang, Y., Beardsley, R. C., Lai, Z., Qi, J., & Lin, H. (2016). Circulation in the Arctic Ocean: Results from a high-resolution coupled ice-sea nested Global-FVCOM and Arctic-FVCOM system. *Progress in Oceanography*, *141*, 60–80. <https://doi.org/10.1016/j.pocean.2015.12.002>
- Cherkasheva, A., Bracher, A., Melsheimer, C., Köberle, C., Gerdes, R., Nöthig, E. M., et al. (2014). Influence of the physical environment on polar phytoplankton blooms: A case study in the Fram Strait. *Journal of Marine Systems*, *132*, 196–207. <https://doi.org/10.1016/j.jmarsys.2013.11.008>
- Cherkasheva, A., Nöthig, E.-M., Bauerfeind, E., Melsheimer, C., & Bracher, A. (2013). From the chlorophyll a in the surface layer to its vertical profile: A Greenland Sea relationship for satellite applications. *Ocean Science*, *9*(2), 431–445. <https://doi.org/10.5194/os-9-431-2013>
- de Steur, L., Hansen, E., Gerdes, R., Karcher, M., Fahrbach, E., & Holfort, J. (2009). Freshwater fluxes in the East Greenland Current: A decade of observations. *Geophysical Research Letters*, *36*(23), 14485–5. <https://doi.org/10.1029/2009GL041278>
- d’Ovidio, F., De Monte, S., Alvain, S., Dandonneau, Y., & Lévy, M. (2010). Fluid dynamical niches of phytoplankton types. *Proceedings of the National Academy of Sciences of the United States of America*, *107*(43), 18366–18370. <https://doi.org/10.1073/pnas.1004620107>
- d’Ovidio, F., Silvia, D. M., Penna, A. D., Cotté, C., & Guinet, C. (2013). Ecological implications of eddy retention in the open ocean: A Lagrangian approach. *Journal of Physics A Mathematical and Theoretical*, *46*(25), 254023. <https://doi.org/10.1088/1751-8113/46/25/254023>
- Dufois, F., Hardman-Mountford, N. J., Greenwood, J., Richardson, A. J., Feng, M., Herbet, S., & Matear, R. (2014). Impact of eddies on surface chlorophyll in the South Indian Ocean. *Journal of Geophysical Research*, *119*(11), 8061–8077. <https://doi.org/10.1002/2014JC010164>

- Dupont, F., Higginson, S., Bourdallé-Badie, R., Lu, Y., Roy, F., Smith, G. C., & Davidson, F. (2015). A high-resolution ocean and sea-ice modelling system for the Arctic and North Atlantic oceans. *Geoscientific Model Development*, 8(5), 1577–1594. <https://doi.org/10.5194/gmd-8-1577-2015>
- Fadeev, E., Wietz, M., von Appen, W.-J., Iversen, M. H., Nöthig, E.-M., Engel, A., & Boetius, A. (2021). Submesoscale physicochemical dynamics directly shape bacterioplankton community structure in space and time. *Limnology & Oceanography*, 66. <https://doi.org/10.1002/lno.11799>
- Frajka-Williams, E., Rhines, P. B., & Eriksen, C. C. (2009). Physical controls and mesoscale variability in the Labrador Sea spring phytoplankton bloom observed by Seaglider. *Deep-Sea Research*, 56(12), 2144–2161. <https://doi.org/10.1016/j.dsr.2009.07.008>
- Friedlingstein, P., O'Sullivan, M., Jones, M. W., Andrew, R. M., Hauck, J., Olsen, A., & Zaehle, S. (2020). Global carbon budget 2020. *Earth System Science Data*, 12(4), 3269–3340. <https://doi.org/10.5194/essd-12-3269-2020>
- Garcia, H. E., Locarnini, R. A., Boyer, T. P., & Antonov, J. I. (2006). Volume 4: Nutrients (phosphate, nitrate, silicate). In S. Levitus (Ed.), *World ocean atlas 2005* (p. 396). Washington, D.C.: NOAA Atlas NESDIS, U.S. Government Printing Office.
- Gascard, J. C., Kergomard, C., Jeannin, P. F., & Fily, M. (1988). Diagnostic study of the Fram Strait marginal ice zone during summer from 1983 and 1984 Marginal Ice Zone Experiment Lagrangian observations. *Journal of Geophysical Research*, 93(C4), 3613–3641. <https://doi.org/10.1029/JC093iC04p03613>
- Gaube, P., Chelton, D. B., Strutton, P. G., & Behrenfeld, M. J. (2013). Satellite observations of chlorophyll, phytoplankton biomass, and Ekman pumping in nonlinear mesoscale eddies. *Journal of Geophysical Research*, 118(12), 6349–6370. <https://doi.org/10.1002/2013jc009027>
- Geider, R. J., MacIntyre, H. L., & Kana, T. M. (1998). A dynamic regulatory model of phytoplankton acclimation to light, nutrients, and temperature. *Limnology & Oceanography*, 43(4), 679–694. <https://doi.org/10.4319/lno.1998.43.4.0679>
- Gentleman, W., Leising, A., Frost, B., Strom, S., & Murray, J. (2003). Functional responses for zooplankton feeding on multiple resources: A review of assumptions and biological dynamics. *Deep-Sea Research*, 50(22–26), 2847–2875. <https://doi.org/10.1016/j.dsr.2003.07.001>
- Godø, O. R., Samuelsen, A., Macaulay, G. J., Patel, R., Hjøllø, S. S., Horne, J., & Johannessen, J. A. (2012). Mesoscale eddies are oases for higher trophic marine life. *PLoS One*, 7(1), e30161. <https://doi.org/10.1371/journal.pone.0030161>
- Hattermann, T., Isachsen, P. E., von Appen, W.-J., Albretsen, J., & Sundfjord, A. (2016). Eddy-driven recirculation of Atlantic water in Fram Strait. *Geophysical Research Letters*, 43(7), 3406–3414. <https://doi.org/10.1002/2016gl068323>
- Hauck, J., Zeising, M., Le Quéré, C., Gruber, N., Bakker, D. C., Bopp, L., & Séférian, R. (2020). Consistency and challenges in the ocean carbon sink estimate for the Global Carbon Budget. *Frontiers in Marine Science*, 7, 852. <https://doi.org/10.3389/fmars.2020.571720>
- Hausmann, U., McGillicuddy, D. J., Jr, & Marshall, J. (2017). Observed mesoscale eddy signatures in southern ocean surface mixed-layer depth. *Journal of Geophysical Research*, 122(1), 617–635. <https://doi.org/10.1002/2016JC012225>
- Isern-Fontanet, J., García-Ladona, E., & Font, J. (2006). Vortices of the mediterranean sea: An altimetric perspective. *Journal of Physical Oceanography*, 36(1), 87–103. <https://doi.org/10.1175/JPO2826.1>
- Johannessen, J. A., Johannessen, O. M., Svendsen, E., Shuchman, R., Manley, T., Campbell, W. J., & Van Leer, J. (1987). Mesoscale eddies in the Fram Strait marginal ice zone during the 1983 and 1984 Marginal Ice Zone Experiments. *Journal of Geophysical Research*, 92(C7), 6754–6772. <https://doi.org/10.1029/JC092iC07p06754>
- Kouketsu, S., Tomita, H., Oka, E., Hosoda, S., Kobayashi, T., & Sato, K. (2011). The role of meso-scale eddies in mixed layer deepening and mode water formation in the western North Pacific. *New developments in mode-water research* (pp. 59–73). Springer. https://doi.org/10.1007/978-4-431-54162-2_5
- Kozlov, I. E., Artamonova, A. V., Manucharyan, G. E., & Kubryakov, A. A. (2019). Eddies in the Western Arctic Ocean from spaceborne SAR observations over open ocean and marginal ice zones. *Journal of Geophysical Research*, 124(9), 6601–6616. <https://doi.org/10.1029/2019JC015113>
- Large, W. G., & Yeager, S. G. (2008). The global climatology of an interannually varying air–sea flux data set. *Climate Dynamics*, 33(2–3), 341–364. <https://doi.org/10.1007/s00382-008-0441-3>
- Ledwell, J. R., McGillicuddy, D. J., Jr, & Anderson, L. A. (2008). Nutrient flux into an intense deep chlorophyll layer in a mode-water eddy. *Deep Sea Research Part II: Topical Studies in Oceanography*, 55(10–13), 1139–1160. <https://doi.org/10.1016/j.dsr.2008.02.005>
- Lehahn, Y., d'Ovidio, F., Lévy, M., & Heifetz, E. (2007). Stirring of the northeast Atlantic spring bloom: A Lagrangian analysis based on multisatellite data. *Journal of Geophysical Research*, 112(C8). <https://doi.org/10.1029/2006JC003927>
- Lester, C. W., Wagner, T. J. W., McNamara, D. E., & Cape, M. R. (2020). The influence of meltwater on phytoplankton blooms near the sea-ice edge. *Geophysical Research Letters*, 48, e2020GL091758. <https://doi.org/10.1029/2020GL091758>
- Lévy, M., Jahn, O., Dutkiewicz, S., & Follows, M. J. (2014). Phytoplankton diversity and community structure affected by oceanic dispersal and mesoscale turbulence. *Limnology & Oceanography*, 4(1), 67–84. <https://doi.org/10.1215/21573689-2768549>
- Levy, M., & Klein, P. (2004). Does the low frequency variability of mesoscale dynamics explain a part of the phytoplankton and zooplankton spectral variability? *Proceedings: Mathematical, Physical and Engineering Sciences*, 460(2046), 1673–1687. <https://doi.org/10.1098/rspa.2003.1219>
- Liu, Y., Röttgers, R., Ramírez-Pérez, M., Dinter, T., Steinmetz, F., Nöthig, E.-M., & Bracher, A. (2018). Underway spectrophotometry in the Fram Strait (European Arctic Ocean): A highly resolved chlorophyll a data source for complementing satellite ocean color. *Optics Express*, 26(14), A678–A696. <https://doi.org/10.1364/OE.26.00A678>
- Mahadevan, A. (2016). The impact of submesoscale physics on primary productivity of plankton. *Annual Review of Marine Science*, 8(1), 161–184. <https://doi.org/10.1146/annurev-marine-010814-015912>
- Mahadevan, A., D'Asaro, E., Lee, C., & Perry, M. J. (2012). Eddy-driven stratification initiates North Atlantic spring phytoplankton blooms. *Science*, 337(6090), 54–58. <https://doi.org/10.1126/science.1218740>
- Marchese, C. (2018). *L'influence de l'environnement physique sur les floraisons du phytoplancton aux hautes latitudes: Une perspective satellitaire (Unpublished doctoral dissertation)* (p. 176). Université du Québec à Rimouski.
- Martin, A. P., & Richards, K. J. (2001). Mechanisms for vertical nutrient transport within a north atlantic mesoscale eddy. *Deep Sea Research Part II: Topical Studies in Oceanography*, 48(4–5), 757–773. [https://doi.org/10.1016/S0967-0645\(00\)00096-5](https://doi.org/10.1016/S0967-0645(00)00096-5)
- Martin, A. P., & Srokosz, M. A. (2002). Plankton distribution spectra: Inter-size class variability and the relative slopes for phytoplankton and zooplankton. *Geophysical Research Letters*, 29(24). <https://doi.org/10.1029/2002GL015117>
- Maure, E. R., Ishizaka, J., Sukigara, C., Mino, Y., Aiki, H., Matsuno, T., & Gomes, H. R. (2017). Mesoscale eddies control the timing of spring phytoplankton blooms: A case study in the Japan Sea. *Geophysical Research Letters*, 44(21). <https://doi.org/10.1002/2017GL074359>
- McGillicuddy, D. J., Johnson, R., Siegel, D. A., Michaels, A. F., Bates, N. R., & Knap, A. H. (1999). Mesoscale variations of biogeochemical properties in the Sargasso Sea. *Journal of Geophysical Research*, 104(C6), 13381–13394. <https://doi.org/10.1029/1999JC900021>
- McGillicuddy, D. J., Jr (2016). Mechanisms of physical-biological-biogeochemical interaction at the oceanic mesoscale. *Annual Review of Marine Science*, 8(1), 125–159. <https://doi.org/10.1146/annurev-marine-010814-015606>

- McWilliams, J. C. (1985). Submesoscale, coherent vortices in the ocean. *Reviews of Geophysics*, 23(2), 165–182. <https://doi.org/10.1029/RG023i002p00165>
- Nakayama, Y., Timmermann, R., & Hellmer, H. H. (2020). Impact of West Antarctic ice shelf melting on Southern Ocean hydrography. *The Cryosphere*, 14(7), 2205–2216. <https://doi.org/10.5194/tc-14-2205-2020>
- Nishino, S., Kawaguchi, Y., Fujiwara, A., Shiozaki, T., Aoyama, M., Harada, N., & Kikuchi, T. (2018). Biogeochemical anatomy of a cyclonic warm-core eddy in the Arctic Ocean. *Geophysical Research Letters*, 45(20), 1–9. <https://doi.org/10.1029/2018GL079659>
- Nöthig, E.-M., Bracher, A., Engel, A., Metfies, K., Niehoff, B., Peeken, I., & Wurst, M. (2015). Summertime plankton ecology in Fram Strait: A compilation of long- and short-term observations. *Polar Research*, 34. <https://doi.org/10.3402/polar.v34.23349>
- Nöthig, E.-M., Ramondenc, S., Haas, A., Hehemann, L., Walter, A., Bracher, A., & Boetius, A. (2020). Summertime Chlorophyll a and Particulate Organic Carbon Standing Stocks in Surface Waters of the Fram Strait and the Arctic Ocean (1991–2015). *Frontiers in Marine Science*, 7, 1–15. <https://doi.org/10.3389/fmars.2020.00350>
- Nurser, A. J. G., & Bacon, S. (2014). The Rossby radius in the Arctic Ocean. *Ocean Science*, 10(6), 967–975. <https://doi.org/10.5194/os-10-967-2014>
- Okubo, A. (1970). Horizontal dispersion of floatable particles in the vicinity of velocity singularities such as convergences. *Deep sea research and oceanographic abstracts* (pp. 445–454). [https://doi.org/10.1016/0011-7471\(70\)90059-8](https://doi.org/10.1016/0011-7471(70)90059-8)
- Olita, A., Sparnocchia, S., Cusi, S., Fazioli, L., Sorgente, R., Tintoré, J., & Ribotti, A. (2014). Observations of a phytoplankton spring bloom onset triggered by a density front in NW Mediterranean. *Ocean Science*, 10(4), 657–666. <https://doi.org/10.5194/os-10-657-2014>
- Omand, M. M., D'Asaro, E. A., Lee, C. M., Perry, M. J., Briggs, N., Cetinić, I., & Mahadevan, A. (2015). Eddy-driven subduction exports particulate organic carbon from the spring bloom. *Science*, 348(6231), 222–225. <https://doi.org/10.1126/science.1260062>
- Pnyushkov, A., Polyakov, I. V., Padman, L., & Nguyen, A. T. (2018). Structure and dynamics of mesoscale eddies over the Laptev Sea continental slope in the Arctic Ocean. *Ocean Science*, 14(5). <https://doi.org/10.5194/os-14-1329-2018>
- Ramachandran, S., Tandon, A., & Mahadevan, A. (2014). Enhancement in vertical fluxes at a front by mesoscale-submesoscale coupling. *Journal of Geophysical Research*, 119(12), 8495–8511. <https://doi.org/10.1002/2014JC010211>
- Randelhoff, A., Reigstad, M., Chierici, M., Sundfjord, A., Ivanov, V., Cape, M., & Kristiansen, S. (2018). Seasonality of the physical and biogeochemical hydrography in the inflow to the Arctic Ocean through Fram Strait. *Frontiers in Marine Science*, 5, 224. <https://doi.org/10.3389/fmars.2018.00224>
- Rey, F., Noji, T. T., & Miller, L. A. (2000). Seasonal phytoplankton development and new production in the central Greenland Sea. *Sarsia*, 85(4), 329–344. <https://doi.org/10.1080/00364827.2000.10414584>
- Rohr, T., Harrison, C., Long, M. C., Gaube, P., & Doney, S. C. (2020). Eddy-modified iron, light, and phytoplankton cell division rates in the simulated Southern Ocean. *Global Biogeochemical Cycles*, 34(6), e2019GB006380. <https://doi.org/10.1029/2019GB006380>
- Samuelson, A., Hjøllo, S. S., Johannessen, J. A., & Patel, R. (2012). Particle aggregation at the edges of anticyclonic eddies and implications for distribution of biomass. *Ocean Science*, 8(3), 389–400. <https://doi.org/10.5194/os-8-389-2012>
- Schourup-Kristensen, V., Sidorenko, D., Wolf-Gladrow, D. A., & Völker, C. (2014). A skill assessment of the biogeochemical model REcoM2 coupled to the Finite Element Sea-Ice Ocean Model (FESOM 1.3). *Geoscientific Model Development*, 7(6), 2769–2802. <https://doi.org/10.5194/gmd-7-2769-2014>
- Schourup-Kristensen, V., Wekerle, C., Wolf-Gladrow, D. A., & Völker, C. (2018). Arctic Ocean biogeochemistry in the high resolution FESOM 1.4-REcoM2 model. *Progress in Oceanography*, 168, 65–81. <https://doi.org/10.1016/j.pocean.2018.09.006>
- Sidorenko, D., Danilov, S., Fofonova, V., Cabos, W., Koldunov, N., Scholz, P., & Wang, Q. (2020). AMOC, watermass transformations and their responses to changing resolution in the finite-volume sea ice-ocean model. *Journal of Advances in Modeling Earth Systems*, 12. <https://doi.org/10.1029/2020MS002317>
- Soltwedel, T., Bauerfeind, E., Bergmann, M., Bracher, A., Budaeva, N., Busch, K., & Klages, M. (2016). Natural variability or anthropogenically-induced variation? Insights from 15 years of multidisciplinary observations at the arctic marine LTER site HAUSGARTEN. *Ecological Indicators*, 65, 89–102. <https://doi.org/10.1016/j.ecolind.2015.10.001>
- Song, H., Long, M. C., Gaube, P., Frenger, I., Marshall, J., & McGillicuddy, D. J. (2018). Seasonal variation in the correlation between anomalies of sea level and chlorophyll in the Antarctic Circumpolar Current. *Geophysical Research Letters*, 45(10), 5011–5019. <https://doi.org/10.1029/2017GL076246>
- Sverdrup, H. U. (1953). On conditions for the vernal blooming of phytoplankton. *ICES Journal of Marine Science*, 18(3), 287–295. <https://doi.org/10.1093/icesjms/18.3.287>
- Teigen, S. H., Nilsen, F., & Gjevik, B. (2010). Barotropic instability in the West Spitsbergen Current. *Journal of Geophysical Research*, 115(C7), C07012. <https://doi.org/10.1029/2009JC005996>
- Teigen, S. H., Nilsen, F., Skogseth, R., Gjevik, B., & Beszczynska-Møller, A. (2011). Baroclinic instability in the West Spitsbergen Current. *Journal of Geophysical Research*, 116(C7), C07012. <https://doi.org/10.1029/2011JC006974>
- Tekman, M. B., Wekerle, C., Lorenz, C., Primpke, S., Hasemann, C., Gerdt, G., & Bergmann, M. (2020). Tying up loose ends of microplastic pollution in the arctic: Distribution from the sea surface through the water column to deep-sea sediments at the HAUSGARTEN observatory. *Environmental Science & Technology*, 54(7), 4079–4090. <https://doi.org/10.1021/acs.est.9b06981>
- Timmermann, M.-L., & Marshall, J. (2020). Understanding Arctic Ocean circulation: A review of ocean dynamics in a changing climate. *Journal of Geophysical Research*, 125(4). <https://doi.org/10.1029/2018JC014378>
- Torres-Valdés, S., Tsubouchi, T., Bacon, S., Naveira Garabato, A. C., Sanders, R., McLaughlin, F. A., & Whitley, T. E. (2013). Export of nutrients from the Arctic Ocean. *Journal of Geophysical Research*, 118(4), 1625–1644. <https://doi.org/10.1002/jgrc.20063>
- Uchida, T., Balwada, D., Abernathy, R. P., McKinley, G. A., Smith, S. K., & Lévy, M. (2020). Vertical eddy iron fluxes support primary production in the open Southern Ocean. *Nature Communications*, 11, 1–8. <https://doi.org/10.1038/s41467-020-14955-0>
- von Appen, W.-J., Schauer, U., Hattermann, T., & Beszczynska-Möller, A. (2016). Seasonal cycle of mesoscale instability of the West Spitsbergen Current. *Journal of Physical Oceanography*, 46(4), 1231–1254. <https://doi.org/10.1175/JPO-D-15-0184.1>
- von Appen, W.-J., Strass, V. H., Bracher, A., Xi, H., Hörstmann, C., Iversen, M. H., & Waite, A. M. (2020). High-resolution physical-biogeochemical structure of a filament and an eddy of upwelled water off northwest Africa. *Ocean Science*, 16(1), 253–270. <https://doi.org/10.5194/os-16-253-2020>
- von Appen, W.-J., Wekerle, C., Hehemann, L., Schourup-Kristensen, V., Konrad, C., & Iversen, M. H. (2018). Observations of a submesoscale cyclonic filament in the marginal ice zone. *Geophysical Research Letters*, 47(7). <https://doi.org/10.1029/2018GL077897>
- Wang, Q., Danilov, S., Jung, T., Kaleschke, L., & Wernecke, A. (2016). Sea ice leads in the Arctic Ocean: Model assessment, interannual variability and trends. *Geophysical Research Letters*, 43(13), 7019–7027. <https://doi.org/10.1002/2016GL068696>

- Wang, Q., Danilov, S., Sidorenko, D., Timmermann, R., Wekerle, C., Wang, X., & Schröter, J. (2014). The Finite Element Sea Ice-Ocean Model (FESOM) v1.4: Formulation of an ocean general circulation model. *Geoscientific Model Development*, 7(2), 663–693. <https://doi.org/10.5194/gmd-7-663-2014>
- Watanabe, E., Onodera, J., Harada, N., Honda, M. C., Kimoto, K., Kikuchi, T., & Kishi, M. J. (2014). Enhanced role of eddies in the Arctic marine biological pump. *Nature Communications*, 5, 1–9. <https://doi.org/10.1038/ncomms4950>
- Weiss, J. (1991). The dynamics of enstrophy transfer in two-dimensional hydrodynamics. *Physica D*, 48(2–3), 273–294. [https://doi.org/10.1016/0167-2789\(91\)90088-Q](https://doi.org/10.1016/0167-2789(91)90088-Q)
- Wekerle, C., Hattermann, T., Wang, Q., Crews, L., von Appen, W.-J., & Danilov, S. (2020). Properties and dynamics of mesoscale eddies in Fram Strait from a comparison between two high-resolution ocean-sea ice models. *Ocean Science*, 16(5), 1225–1246. <https://doi.org/10.5194/os-16-1225-2020>
- Wekerle, C., Wang, Q., Danilov, S., Schourup-Kristensen, V., von Appen, W.-J., & Jung, T. (2017). Atlantic Water in the Nordic Seas: Locally eddy-permitting ocean simulation in a global setup. *Journal of Geophysical Research*, 122(2), 914–940. <https://doi.org/10.1002/2016JC012121>
- Wekerle, C., Wang, Q., von Appen, W.-J., Danilov, S., Schourup-Kristensen, V., & Jung, T. (2017). Eddy-resolving simulation of the Atlantic Water circulation in the Fram Strait with focus on the seasonal cycle. *Journal of Geophysical Research*, 122(11), 8385–8405. <https://doi.org/10.1002/2017JC012974>
- Wulff, T., Bauerfeind, E., & von Appen, W.-J. (2016). Physical and ecological processes at a moving ice edge in the Fram Strait as observed with an AUV. *Deep-Sea Research*, 115(C), 253–264. <https://doi.org/10.1016/j.dsr.2016.07.001>
- Xu, L., Xie, S.-P., Liu, Q., Liu, C., Li, P., & Lin, X. (2017). Evolution of the North Pacific subtropical mode water in anticyclonic eddies. *Journal of Geophysical Research*, 122(12), 10118–10130. <https://doi.org/10.1002/2017JC013450>
- Zawada, D. G., Zaneveld, J. R. V., Boss, E., Gardner, W. D., Richardson, M. J., & Mishonov, A. V. (2005). A comparison of hydrographical and optically derived mixed layer depths. *Journal of Geophysical Research*, 110(C11), 63–13. <https://doi.org/10.1029/2004JC002417>